Journal of Drug Delivery Science and Technology 101 (2024) 106215

Contents lists available at ScienceDirect

Journal of Drug Delivery Science and Technology

journal homepage: www.elsevier.com/locate/jddst

Gold nanoparticles for photothermal therapy – Influence of experimental conditions on the properties of resulting AuNPs

Mariana Neves Amaral [a,b], Daniela Nunes [c], Elvira Fortunato [c], Rodrigo Martins [c], Carla Rodrigues [d], Pedro Faísca [e], Hugo Alexandre Ferreira [b], João M.P. Coelho [b], M. Manuela Gaspar [a,b], Catarina Pinto Reis [a,b,*]

[a] Research Institute for Medicines (iMed.ULisboa), Faculty of Pharmacy, Universidade de Lisboa, Av. Professor Gama Pinto, 1649-003, Lisboa, Portugal
[b] Instituto de Biofísica e Engenharia Biomédica (IBEB), Faculdade de Ciências, Universidade de Lisboa, Campo Grande, 1749-016, Lisboa, Portugal
[c] Department of Materials Science, NOVA School of Science and Technology, Campus de Caparica, i3N/CENIMAT, 2829-516, Caparica, Portugal
[d] REQUIMTE/CQFB, Departamento de Química, Faculdade de Ciências e Tecnologia, Universidade Nova de Lisboa, 2829-516, Caparica, Portugal
[e] CECAV- Centro de Ciência Animal e Veterinária-Faculdade de Medicina Veterinária, Universidade Lusófona, Centro Universitário de Lisboa, Campo Grande 376, 1749-024, Lisbon, Portugal

ARTICLE INFO

Keywords:
Gold nanoparticles
Gold nanoflowers
Photothermal therapy
Cancer
Novel therapies
Hyperthermia
Photothermal agents

ABSTRACT

Gold nanoparticles (AuNPs)-mediated Photothermal Therapy (PTT) is a minimally-invasive therapeutic approach that uses AuNPs to convert light into heat, leading to the thermal ablation of tumors. Thus, the efficacy of this strategy strongly relies on the photothermal conversion potential of AuNPs. The ability to convert light into heat can be enhanced by tuning the physicochemical and optical properties of AuNPs. This can be achieved by changing the conditions of AuNP's synthesis, such as the order of addition of reagents. The present work entails to explore how varying the order of reagents addition modulates the properties of AuNPs, particularly enhancing the photothermal conversion potential of the resulting AuNPs and consequently, improving PTT efficacy. For this, eleven different AuNPs' nanoformulations were synthetized following different sequences of addition of reagents. These nanoformulations were characterized regarding their physicochemical properties namely size, surface charge, gold concentration, surface morphology and maximum absorbance wavelength. In addition, their thermal activation profiles were determined *in vitro*. Furthermore, the biocompatibility of different nanoformulations was also assessed. Three nanoformulations, with the most favorable photothermal activation profiles (AuNPs 2, 3 and 7), were then selected for preliminary *in vitro* safety and efficacy assays using a panel of cell lines. These three nanoformulations were deemed safe *in vitro* at the tested concentrations. At 250 μM of gold content, and after an incubation period of 4 h, followed by 5 min irradiation with a laser emitting at 808 nm (7.96 W/cm^2), AuNPs 7 significantly reduced the cell viability of all cancer cell lines tested (MCF-7, HCT-116 and A375) by $\geq$ 45 %. However, such cytotoxic effect was not observed for the human keratinocyte cell line (HaCat), thus demonstrating its specificity towards cancer cells. Overall, the results herein presented reinforce that the order of reagents addition is highly important for achieving adequate AuNPs for PTT.

1. Introduction

Photothermal therapy (PTT) entails using a light source to increase the temperature of tissues. It offers a high spatiotemporal control with reduced side effects [1–5]. However, to efficiently increase the temperature to the point in which cancer cells undergo hyperthermia-mediated cell death, light-absorbing gold nanoparticles (AuNPs) can be used [6–15]. Upon administration and accumulation in the tumour, AuNPs will absorb irradiated light and convert it into heat at the accumulation site. Out of the light spectrum, near-infrared (NIR) wavelengths (780–3000 nm, according to ISO 20473:2007) present advantages for PTT application, i.e., higher tissue penetration capacity, less photodamage due to being less energetic, and lower absorption and scattering before reaching the AuNPs [16–18]. The efficacy of AuNPs-mediated PTT is dependent on different factors such as tumour depth and photothermal conversion efficacy of the AuNPs. Furthermore,

* Corresponding author. Faculty of Pharmacy, Universidade de Lisboa, Av. Professor Gama Pinto, 1649-003, Lisboa, Portugal.
E-mail address: catarinareis@ff.ulisboa.pt (C.P. Reis).

https://doi.org/10.1016/j.jddst.2024.106215
Received 29 February 2024; Received in revised form 20 August 2024; Accepted 17 September 2024
Available online 18 September 2024

to promote high photothermal conversion, the wavelength in which the AuNPs absorb must ideally be the wavelength at which the laser emits [2,19]. This is due to the Surface Plasmon Resonance (SPR) effect: upon AuNPs being irradiated by a light source in the characteristic SPR wavelength of that AuNPs, free electrons will resonate at the AuNPs' surface until the maximum amplitude of oscillation, SPR, is reached. When the nonradiative decay of this oscillation occurs, light energy is converted into thermal energy (photothermal conversion) [17].

The optical properties of AuNPs can be tuned to manipulate their SPR wavelength by changing AuNPs' physicochemical properties (i.e., size, shape, etc.) and/or by modifying their surfaces. This surface modification can include the addition of surface coatings, as is the case of keratin and hyaluronic and oleic acids mixture [20–22]. Furthermore, ligands can be added to the surface of AuNPs in order to increase their targeting to cancer cells, which can also change the optical properties of the final AuNPs [23,24]. Moreover, the reduction of the gold salt depends on the type of the reducing and stabilizing agents used [25].

The most commonly used method for the synthesis of AuNPs is the Turkevich method, in which gold (III) chloride trihydride ($HAuCl_4.3H_2O$) is reduced by sodium citrate. The effects of varying the order of addition of reagents used in this method (direct method, sodium citrate added to a $HAuCl_4.3H_2O$ solution; or indirect method, $HAuCl_4.3H_2O$ added to a sodium citrate solution) have been previously studied [26]. By inverting the order of reagent addition, the SPR peak of the resultant AuNPs suffered a strong blue shift and presented smaller mean sizes compared to when AuNPs were produced with the standard order of reagent addition [26], indicating that varying the order of reagents addition during the synthesis of AuNPs might change the properties of the resulting AuNPs.

To the best of our knowledge, the changes resulting from varying the sequence of reagent addition have only been studied in the most common methods of AuNPs synthesis (i.e., Turkevich method). In our case, two different reducing agents (ascorbic acid and rosmarinic acid) were used to reduce the $HAuCl_4.3H_2O$ in the presence of silver nitrate ($AgNO_3$). The standard method includes the following order: $AgNO_3$; ascorbic acid; and finally rosmarinic acid. Thus, this work aims to explore how solely changing the order of the reagents addition (used in previous work to synthetize AuNPs [8]) tunes the optical and physicochemical properties and, consequently, photothermal conversion efficiency, safety and efficacy of AuNPs. Herein, different sequences of reagents addition were studied, with and without the presence of $AgNO_3$. Eleven different sequences were tested, and compared with the original AuNPs (AuNPs 1). All nanoformulations were fully characterized in terms of their physicochemical and optical properties. The AuNPs with the most promising characteristics with emphasis on SPR peak, absorbance at 808 nm, and thermal activation as well as biocompatibility, were selected for *in vitro* safety and efficacy studies.

2. Materials and methods

2.1. Materials

2.1.1. Reagents

Gold (III) chloride trihydrate ($HAuCl_4.3H_2O$), L-Ascorbic Acid (ascorbic acid), Silver Nitrate ($AgNO_3$), Rosmarinic Acid and 3-(4,5-dimethylthiazol-2-yl)-2,5-diphenyltetrazolium bromide (MTT) were acquired from Sigma-Aldrich (St. Louis, MO, USA). Dulbecco's modified Eagle's medium (DMEM), foetal bovine serum (FBS), penicillin and streptomycin were supplied from Gibco, Thermo Fisher Scientific, Waltham, MA, USA). Artificial seawater salt and *Artemia salina* eggs were provided from JBL GmbH & Co. (Neuhofen, Germany). Water Milli-Q was provided by Merck Millipore System (Burlington, MA, USA). All other chemicals were of analytical grade.

2.1.2. Cell lines and cell culture

All cells were grown in accordance with the supplier's (ATCC) instructions. The commercialized human cell lines of breast cancer (MCF-7), colon cancer (HCT-116), melanoma (A375) and keratinocytes (HaCat) were maintained in Dulbecco's modified Eagle's medium (DMEM), completed with 10 % foetal bovine serum (FBS), 100 IU/mL of penicillin and 100 μg/mL of streptomycin. The cell lines were kept in a humidified chamber at a temperature of 37 °C and an atmosphere of 5 % CO_2. The cells in culture were maintained every 2–3 days, and when a confluence of 80 % was attained, the medium was changed.

2.2. Methods

2.2.1. Preparation of AuNPs

Eleven nanoformulations of AuNPs were prepared by modifying a method previously published [6–8,11]. The mentioned method is based on using ascorbic acid and rosmarinic acid, to reduce the $HAuCl_4.3H_2O$ in the presence of $AgNO_3$. The eleven different nanoformulations developed in this work were prepared by changing the order in which the mentioned reagents were added (Fig. 1), but maintaining the concentrations and volumes used. Besides varying the reagents order, in some of the nanoformulations $AgNO_3$ was not added (i.e., AuNPs 2, 4, 8, 9, 10 and 11).

After addition of the aqueous solutions in the respective order, the mixture was continuously stirred in a magnetic stirrer (Heidolph magnetic stirrer hotplate MR3001, Heidolph Instruments, Schwabach, Germany) at 800 rpm, for 15 min. After being synthesized, the AuNPs were recovered by centrifuging the suspension at 1520×*g*, for 20 min (Beckman Instruments Centrifuge, Inc., Brea, CA, USA). The supernatant was discarded and the pellet containing the AuNPs was suspended in Milli-Q water.

Inductively Coupled Plasma-Optical Emission Spectrometry (ICP-OES, Ultima, Horiba Jobin-Yvon, Longjumeau, France) was used to determine the experimental concentration of elemental gold (Au) present in each nanoformulations. Prior to analysis, each nanoformulation was digested using nitric acid (HNO_3, 69 % for trace metal analysis, PanReac AppliChem, Barcelona, Spain).

2.2.2. Physicochemical characterization

2.2.2.1. Mean size and polydispersity index (PdI). All nanoformulations were characterized regarding their mean size, polydispersity index (PdI), and surface charge. For these characterizations, the different nanoformulations (at 125 μM of gold) were diluted in Milli-Q water (1:10, v/v, Milli-Q water:AuNPs), to analyze mean size and PdI, and diluted in PBS (1:10, v/v, PBS) to determine zeta potential. Mean size and PdI were analyzed by Dynamic Light Scattering (DLS), using a Zetasizer Nano S (Malvern Instruments, Malvern, UK), and surface charge was characterized by determining zeta potential, through Electrophoretic Mobility Assay, using a Zetasizer Nano Z (Malvern Instruments, Malvern, UK). All measurements were performed ≥3 times.

2.2.2.2. Morphology assessment. Morphology of the different nanoformulations (1-11) was assessed using Scanning Electron Microscopy (SEM). For SEM observations, small droplets (20 μL) of aqueous suspensions of AuNPs were placed on silicon substrates and left to dry at room temperature, and SEM images were acquired using a Hitachi Regulus 8220 Scanning Electron Microscope (Hitachi, Mito, Japan). The images were digitally recorded.

2.2.2.3. Determination of absorbance spectra. The maximum absorbance peak (Abs_{max}) and absorbance at 808 nm (Abs_{808nm}) for the AuNPs were determined by scanning the absorbance spectrum (between 400 and 1000 nm) of all nanoformulations using a UV–Vis spectrophotometer (Shimadzu UV-1280, Shimadzu, Corp., Kyoto, Japan). All measurements were performed in triplicate.

The molar extinction coefficient, $\varepsilon(\lambda)$, of the different AuNP

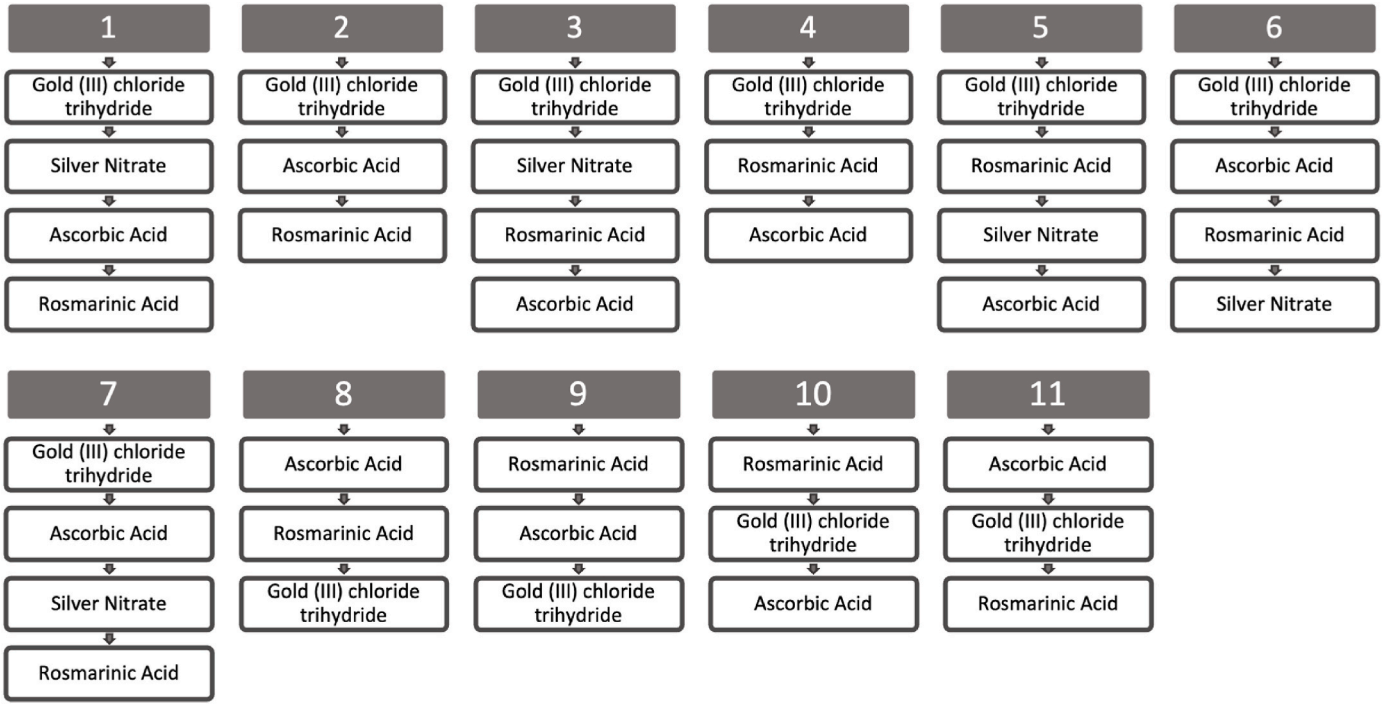

Fig. 1. Order in which the reagents were added for the preparation of different eleven AuNPs' nanoformulations.

nanoformulations (1-11) was determined using the Lambert-Beer Law, following Equation (1) [27]:

$$A(\lambda) = \varepsilon(\lambda) L C_{AuNPs}, \quad (1)$$

where A(λ) is the optical density at a certain wavelength, $\varepsilon(\lambda)$ is the molar extinction coefficient for the same wavelength, L is the path length crossed by the incident light passing through the suspension, in cm, and C_{AuNPs} is the concentration of AuNPs in each suspension, in molar (M). C_{AuNPs} can be determined following Equation (2) [27]:

$$C_{AuNPs} = \frac{C_{Au} \times NA}{N_{Au}}, \quad (2)$$

in which C_{Au} is the concentration of gold atoms present in each AuNPs' suspension, as determined by ICP-OES, NA is the Avogadro constant, and N_{Au} is the number of gold atoms per AuNP. In turn, taking into account that Au (III) prefers a coordination number of 4, N_{Au} can be estimated following Equation (3) [27]:

$$N_{Au} = 4 \times N_{unit\ cells}, \quad (3)$$

where $N_{unit\ cells}$ of Au represents the number of unit cells in each AuNP and can be calculated following Equation (4) [27]:

$$N_{unit\ cells} = \frac{V_{AuNPs}}{V_{unit\ cells}}, \quad (4)$$

$V_{unit\ cells}$ signifies the volume of a Face-Centered Cubic (FCC) unit cell of Au, of 67.42 Å^3, and V_{AuNPs} denotes the volume of each AuNP. As shown by the morphological analysis, the different AuNPs mostly present spherical-like morphologies, and thus V_{AuNPs} of each nanoformulation were determined by calculating the volume of spheres using the mean diameter of AuNPs determined by DLS [27].

2.2.3. *In vitro thermal activation*

To test the thermal activation of the nanoformulations upon NIR laser irradiation, the AuNPs were incorporated in agar phantoms at a concentration of 125 μM of gold. To prepare the phantoms (Fig. S1), an agar aquous solution was prepared at 1 % (w/v) under magnetic agitation and heat, to promote agar solubilization. After this, 1 mL of the prepared solution was poured into each polystyrene cuvette and left to jellify. To incorporate the nanoformulations in the gelled agar, a centered well was poked in the center gelled agar of the different cuvettes, to which 20 μL of each nanoformulation was added (test phantoms). A black plasticine sphere was added to the well of the positive control phantom, and the well of the negative control phantom was left empty. After the preparation of the wells, another 1 mL of the agar solution was added on top of the wells, and left to jellify, concluding the phantom preparation. Subsequently, a thermocouple (Fluke 52 K/J thermometer, Everett, WA, USA) was immersed in the agar phantoms, approximately at the same distance from the well in each phantom, as shown by Ferreira-Gonçalves et al. [9] allowing to measure the temperature in the agar surrounding the test and control wells. A FC-808-2W Fiber Coupled Laser System (Frankfurt Laser Company, Friedrichsdorf, Hessen Germany) coupled to an FPYL-COL-X collimator (Frankfurt Laser Company, Friedrichsdorf, Hessen Germany) emitting at a wavelength of 808 nm, was used to activate the AuNPs. The different phantoms were irradiated for 10 min each, at an irradiance of 7.96 W/cm^2, and the temperature of the phantoms was assessed every 30 s, and the temperature increment was determined.

2.2.4. *Safety Assessment*

2.2.4.1. Saccharomyces kudriavzevii model. As a preliminary safety assay, the *Saccharomyces kudriavzevii* (ATCC® 2601) model was used [11,28]. The yeast cells were cultured in yeast extract peptone dextrose medium, with 1 % yeast extract, 0.5 % peptone and 2 % glucose, respectively. Disposable cuvettes containing 2 mL of *Saccharomyces kudriavzevii* at a concentration of 1.0×10^7 yeast cells/mL were prepared. Cuvettes containing untreated yeast were used as negative control. The AuNPs' nanoformulations (200 μL) were added to the respective yeast-containing cuvettes at a concentration of 125 μM in terms of gold. After, the cuvettes, kept at 30 °C, were gently mixed and the absorbance was read at 525 nm, using a UV–Vis spectrophotometer (Shimadzu UV-1280, Shimadzu, Corp., Kyoto, Japan) at 0, 1, 2, 4 and 6 h. The concentration of yeast cells was calculated following Equation (5)

in order to plot the growth curve against time:

$$Abs_{525nm} = 6.8219 \times 10^{-8}x + 0.0327, \quad (5)$$

in which Abs_{525nm} is sample absorbance at 525 nm and x is yeast cell concentration (yeast cell/mL). For each sample, growth inhibition was calculated from the linear slope of the logarithmic growth curve. All nanoformulations were tested independently thrice, in triplicates each time.

2.2.4.2. Artemia salina model. *Artemia salina*, also known as brine shrimp, was used to assess the safety in a preliminary *in vivo* model. Firstly, artificial seawater was prepared by mixing regular tap water with commercial seawater salt, according to supplier instructions. The dry *A. salina* cysts were added to the artificial seawater and were left to hatch under aeration and artificial light, for 48 h, at 25–30 °C. After this, 900 μL of artificial seawater, containing 10–15 nauplii, and 100 μL of each of the nanoformulations: all different eleven AuNPs formulations, at 125 μM of gold; 10 % dimethyl sulfoxide (DMSO) as positive control; and artificial seawater as negative control were added to 24-well plates and incubated for 24 h, at 25–30 °C. After that, the dead nauplii were counted. To kill the remaining nauplii, 100 % DMSO was added to all the wells and left to incubate for 2 h, at 25–30 °C. After the total *A. salina* was counted, the mortality (%) was calculated following Equation (6) [4,18]:

$$Mortality\ (\%) = \frac{Dead_{24\ h}}{Dead_{Total}} \times 100, \quad (6)$$

in which $Dead_{24\ h}$ represents the number of dead *A. salina* nauplii 24 h after incubation, and $Dead_{Total}$ represents the total of nauplii present in each well. All nanoformulations were tested independently thrice, with four replicates each time.

2.2.4.3. Immortalized human cell lines. Human keratinocyte cell line (HaCat) and different human cancer cell lines (breast, MCF-7; colon cancer, HCT-116; and melanoma, A375) were used to assess the safety of the three most promising nanoformulations (AuNPs 2, AuNPs 3 and AuNPs 7). Different concentrations of gold (125, 250 and 375 μM) were tested. The day before the incubation of the nanoformulations, each cell line was seeded in 96-well plates at a concentration of 5×10^4 cells/mL, and left to adhere overnight in an atmosphere of 37 °C, 5 % CO_2. The next day, medium was removed, and cells were incubated with all AuNPs, at the above-mentioned concentrations, or with complete medium (negative control), corresponding to 100 % of cell viability, for 24 h. The viability of the different cell lines was evaluated using the 3-(4,5-dimethylthiazol-2-yl)-2,5-diphenyltetrazolium bromide (MTT) assay [4,6–10,27,29]. For this, the medium was removed and the cells were washed twice with PBS (pH 7.4, USP32). Subsequently, 50 μL of the MTT (0.5 mg/mL in incomplete DMEM) (Sigma-Aldrich, St. Louis, MO, USA) was added and left to incubate until formazan crystals were formed (2–3 h, at 37 °C, 5 % CO_2). Then, crystals were solubilized using DMSO, and absorbances were measured at 570 nm using a BioTekTM EL × 800TM Absorbance Microplate Reader (Fisher Scientific, NH, USA). The absorbance of the control, cells in the presence of complete medium, represent 100 % cell viability. Results were determined following Equation (7):

$$Cell\ Viability\ (\%) = \frac{Abs_{test\ group}}{Abs_{Control}} \times 100 \quad (7)$$

2.2.5. Efficacy assessment

The same human keratinocytes (HaCat) and cancer (HCT-116, A375 and MCF-7) were used to assess the efficacy of these three promising nanoformulations at 250 μM, upon activation (i.e., irradiation) by laser. Each cell line was seeded in 96-well plates at a concentration of 5×10^4 cells/mL, and allowed to adhere overnight in an atmosphere of 37 °C, 5 % CO_2. Wells intended to be irradiated were separated by one empty well in all directions to avoid eventual collateral scattering or reflection of light from irradiated wells [27]. The next day, medium was removed, and cells were incubated with the different AuNPs, or with complete medium (corresponding to 100 % cell viability) for 4 h [6–10,12,27]. After this incubation period, the AuNP-containing medium was removed and replaced with fresh medium, and the treatment (AuNPs 2, 3 and 7) and laser (without AuNPs) control wells were irradiated at an irradiance of 7.96 W/cm^2 for 5 min [27]. To irradiate, and thus activate the AuNPs, an FC-808-2W Fiber Coupled Laser System (Frankfurt Laser Company, Friedrichsdorf, Hessen Germany) coupled to an FPYL-COL-X collimator (Frankfurt Laser Company, Friedrichsdorf, Hessen Germany) emitting at a wavelength of 808 nm, was used. As for the safety assessment, the viability of the different cell lines was assessed 24 h after irradiation using MTT assay. As in the previous assay, medium was removed from the wells, and cells were washed twice with PBS (pH 7.4), and 50 μL of MTT at a concentration of 0.5 mg/mL in incomplete DMEM was added to all wells. After hydrophobic formazan crystals formation, DMSO was added for solubilization, and absorbances were read at 570 nm using a BioTekTM EL × 800TM Absorbance Microplate Reader (Fisher Scientific, NH, USA). Again, the absorbance of control cells, left untreated, represented 100 % viability. Results are shown as percentage of cell viability, and were calculated following Equation (7), as previously mentioned.

2.2.6. Morphological and elemental characterization of best-performing AuNPs

X-Ray Diffaction (XRD) was performed using a Aeris Benchtop XRD System (Malvern Instruments, Malvern, UK), equipped with a PIXcel1D detector, and using CuKα radiation (λ = 1.540598 Å). XRD data was recorded from 20° to 80° 2θ range, with a step of 0.02° in the Bragg–-Brentano configuration. Simulated AuNPs was indexed considering the JCPDS file No. 04–0784.

The best-performing AuNPs were selected for further characterization. For this, AuNPs 7 were sonicated and a drop of the sample was placed on a lacey-carbon copper grid and left to dry. The scanning transmission electron microscopy (STEM) observations were performed using a Hitachi HF5000 field-emission transmission electron microscope (Hitachi, Mito, Japan), at 200 kV, and included high-angle annular dark field (HAADF) imaging. Hitachi HF5000 field-emission transmission electron microscope is a cold field emission gun TEM/STEM, with a spherical aberration-corrector for the probe, and is equipped with one 100 mm^2 EDS detector from Oxford Instruments (Oxford Instruments, Abingdon, Oxfordshire, UK) [27].

2.2.7. Statistical analysis

All data is presented as mean ± standard deviation (SD), for the referred n. Comparisons of one factor among groups were analyzed using Student's *t*-test (for two groups) or using one-way or two-way ANOVA (for three or more groups). GraphPad Prism 10® (GraphPad Software, San Diego, CA, USA) was used to carry out all analyses, and differences were deemed significant for $p < 0.05$.

3. Results

3.1. Characterization of mean size, polydispersity index (PdI), and surface charge

The resulting eleven AuNPs were characterized regarding their mean size, PdI, surface charge, and concentration of gold (Au) at the end of synthesis concentration, and the results are presented in Table 1. The mean size of the different nanoformulations varied from 121.3 nm, for AuNPs 8, to 215.8 nm, for AuNPs 5, while PdI varied between 0.254 and 0.357, for AuNPs 8 and AuNPs 6, respectively. All eleven AuNP formulations presented a negative surface charge, with zeta potential values ranging from −23 to −30 mV. The concentration of gold salt for

Table 1
Characterization of size (nm), polydispersity index (PdI), surface charge (zeta potential, mV) and gold (Au) concentration (mM) at the end of synthesis of the eleven different nanoformulations. Mean ± SD, n > 3.

AuNPs	Mean size (nm)	PdI	Zeta potential (mV)	[Au] (mM)
1	144.5 ± 52.3	0.330 ± 0.084	−29 ± 3	0.43 ± 0.06
2	184.3 ± 71.1	0.283 ± 0.077	−27 ± 7	0.55 ± 0.02
3	162.7 ± 64.4	0.313 ± 0.073	−26 ± 11	0.49 ± 0.10
4	164.9 ± 45.5	0.285 ± 0.092	−30 ± 2	0.56 ± 0.08
5	215.8 ± 84.9	0.343 ± 0.067	−30 ± 2	0.55 ± 0.09
6	204.6 ± 74.0	0.357 ± 0.147	−23 ± 2	0.63 ± 0.09
7	164.2 ± 39.4	0.354 ± 0.082	−30 ± 2	0.50 ± 0.05
8	121.3 ± 38.8	0.254 ± 0.101	−27 ± 3	0.60 ± 0.04
9	167.0 ± 84.6	0.255 ± 0.143	−29 ± 4	0.64 ± 0.09
10	158.9 ± 57.0	0.317 ± 0.101	−28 ± 3	0.56 ± 0.08
11	143.9 ± 47.7	0.256 ± 0.146	−29 ± 3	0.54 ± 0.15

the different eleven AuNPs was quite similar ranging from 0.43, for AuNPs 1 to 0.64 mM observed for AuNPs 9.

3.2. Morphological analysis

Scanning electron microscopy (SEM) was used to assess the morphology of the eleven AuNP formulations, and representative images of populations (A, C, E, G, I, K, M, O, Q, S and U) and of close-ups of AuNPs (B, D, F, H, J, L, N, P, R, T and V) are presented in Fig. 2. Firstly, it is to note that, although from a general analysis, all AuNPs' formulations exhibited a uniform shape among their populations, nanoformulations 1, 2, 4 and 10 presented a nanoflower-like morphology. When ascorbic acid and rosmarinic acid were sequentially added as the two last reagents, in the presence (AuNPs 1) and absence (AuNPs 2) of $AgNO_3$, the resulting nanoformulations presented a mixed population of small nanoparticles with three subpopulations: AuNPs of larger size, exhibited a nanoflower morphology and a size ~400 nm; planar AuNPs sized ~150 nm; and quasi-spherical AuNPs of smaller size, <50 nm. Planar structures were more prevalent when $AgNO_3$ was included in nanoformulations syntheses (AuNPs 1). The morphology of AuNPs 3, 5, 6 and 7 resembled the nanoflowers with nanosheet aggregations, which can be seen in their isolated non-aggregated form in AuNPs 1 and 2. When the reducing agents were added first, prior to the gold solution, the resulting AuNPs (AuNPs 8–11) presented a more compact and less branched nanoflower morphology, similar to AuNPs 4. This morphology resembles a quasi-spherical shape, presenting short and irregular branches, less pronounced than the branches seen in the other AuNPs nanoflowers.

3.3. Absorbance spectra

To be photoactivated and able to efficiently transform NIR light into heat, the AuNPs must present a maximum absorbance peak or absorb radiation in these wavelengths (NIR, 780–3000 nm). Thus, the absorbance spectra of each of the eleven AuNPs formulations was determined between 400 and 1000 nm (Fig. S2), and the wavelength corresponding to the maximum absorbance peak (λAbs_{max}), of each nanoformulation, was also determined, as shown in Table 2. Also, it is very important for the PTT formulation to present increased absorbance at the wavelength that the NIR laser emits. In this case, the laser used to activate the AuNPs emits at 808 nm, and thus the absorbance at 808 nm (Abs_{808nm}) was also determined (Table 2). The molar extinction coefficient at a certain wavelength, in this case, 808 nm, is a measurement of how strongly the different AuNPs formulations absorb light at this wavelength. The molar extinction coefficient at 808 nm, number of Au atoms per AuNP, and the concentration of AuNPs for each AuNP formulation are also presented in Table 2. Looking at the results regarding Abs_{max}, it is to note that AuNPs 3 and 5 presented significantly different SPR peaks in comparison to the standard AuNP formulation (AuNPs 1), with no nanoformulation presenting Abs_{808nm} significantly superior to AuNPs 1. Moreover, AuNPs 5–8 also presented a significantly higher molar extinction coefficient at the wavelength of interest, 808 nm, with AuNPs 7 presenting the highest molar extinction coefficient at 808 nm amongst all AuNPs.

3.4. In vitro thermal activation

The thermal activation of AuNPs by a NIR laser upon irradiation is a crucial step for PTT, as it relies on the thermal heat generated at a restricted site. To evaluate the thermal activation of the eleven different AuNP formulations, the AuNPs were incorporated into agar phantoms at a concentration of 125 μM of gold, and irradiated with a NIR laser for 10 min, registering the agar's temperature every 30 s. A black plasticine sphere was used as a positive control and an agar phantom, without AuNPs, was used as a negative control, and both controls were irradiated by a NIR laser (808 nm, 5.6 W/cm^2) for 10 min. Results of the temperature increment of the eleven irradiated AuNPs and the controls in function of time are presented in Fig. 3. All nanoformulations resulted in a significant overall temperature increase in comparison to the negative control (agar + laser). Looking at the temperature increment curves for the eleven nanoformulations, it is to note that AuNPs 2, 3 and 7 resulted in the highest increases of temperature in the agar.

To better understand how each AuNP formulation increased the agar's temperature over time (10 min), the temperature increment every 30 s of each AuNP formulation was plotted individually, with the negative control, and is presented in Fig. 4A–K. The AuNP nanoformulation that presented the highest degree of significant temperature increase over the larger number of time points was AuNPs 7, followed by AuNPs 2 and AuNPs 3, underlining the conclusions drawn from Fig. 3. AuNPs 6 and 11 were the ones that resulted in the least statistically significant temperature increase, with AuNPs 11 presenting no statistically significant temperature increases when compared to the negative control for all time points.

3.5. Safety assessment

3.5.1. Saccharomyces kudriavzevii model

Safety was preliminarily evaluated in the *Saccharomyces kudriavzevii* model, a versatile eukaryotic *in vivo* system, by analyzing the growth inhibition of this microorganism when in the presence of the eleven AuNP formulations. For this, *S. kudriavzevii* was incubated with each of the eleven AuNPs for 6 h, and the growth curve was calculated and compared to the growth curve of the negative control, *S. kudriavzevii* in the presence of yeast extract peptone dextrose medium The determined growth inhibition for the eleven AuNPs is presented in Fig. 5. None of the AuNPs formulations inhibited growth when compared to the negative control.

3.5.2. Artemia salina model

Safety of the eleven nanoformulations was also preliminarily assessed *in vivo* using *Artemia salina*, an *in vivo* model commonly used to assess the toxicity of heavy metals and nanoparticles, among others [30]. The nauplii were incubated with the eleven AuNPs at 125 μM of gold, for 24 h, as well as with the negative control (artificial seawater) and positive control (10 % DMSO), and the results are presented in Fig. 6. It is to note that, although nauplii incubated with AuNPs 2 presented mortality, it is still very low (<10 %). Thus, all nanoformulations were considered safe according to the preliminary *in vivo A. salina* mortality assessment.

3.5.3. Immortalized human cell lines

Considering all previous results and particularly the thermal conversion profiles, the safety of the three best nanoformulations (AuNPs 2, 3 and 7) was assessed *in vitro* using the human keratinocyte cell line, HaCat, and the human cancer cell lines MCF-7, HCT-116 and A375. The different cell lines were independently incubated with the three AuNPs formulations for 24 h, at three different concentrations in terms of gold

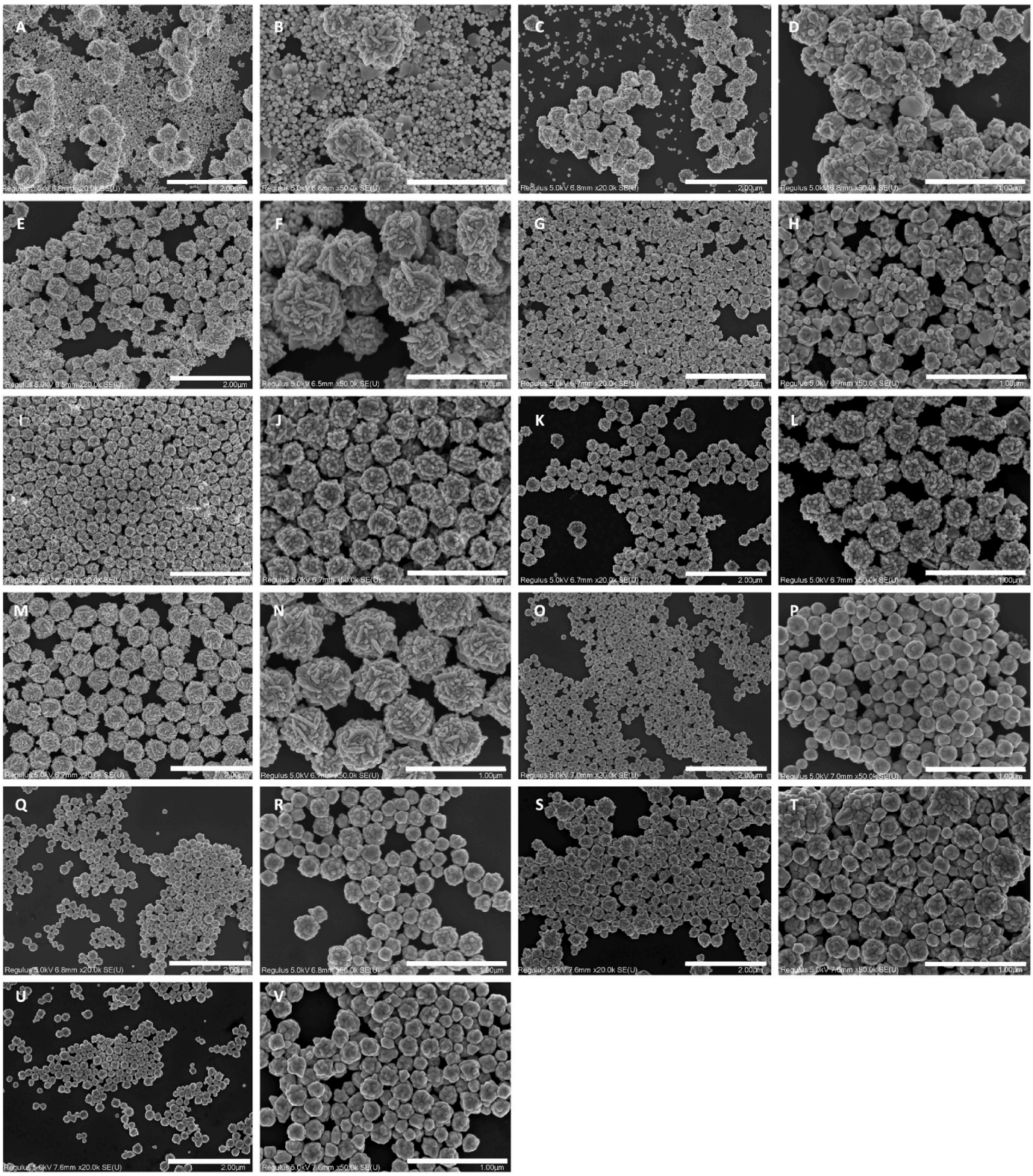

Fig. 2. SEM micrographs of AuNPs 1 (**A,B**), AuNPs 2 (**C,D**), AuNPs 3 (**E,F**), AuNPs 4 (**G,H**), AuNPs 5 (**I,J**), AuNPs 6 (**K,L**), AuNPs 7 (**M,N**), AuNPs 8 (**O,P**), AuNPs 9 (**Q,R**), AuNPs 10 (**S,T**) and AuNPs 11 (**U,V**). Scale bars = 2 μm (**A, C, E, G, I, K, M, O, Q, S** and **U**), and 1 μm (**B, D, F, H, J, L, N, P, R, T** and **V**).

content (125, 250 and 375 μM). Results are presented in Fig. 7. Generally, it is to note that although all nanoformulations slightly induced cell viability changes, this effect was dependent on gold concentration. Nevertheless, cell viability was always above 70 % for all tested concentrations of the three nanoformulations thus demonstrating its safety according to ISO 10993–5:2009(E) [8].

3.6. Preliminary in vitro efficacy assessment

As was for safety, efficacy of the three different nanoformulations

Table 2
Wavelength corresponding to the maximum absorbance peak (λAbs_{max}, nm), absorbance at 808 nm (Abs_{808nm}), number of Au atoms per AuNP, concentration of AuNPs (mM) and molar extinction coefficient at 808 nm (M^{-1} cm^{-1}) of the eleven different AuNPs at a concentration of 125 μM of gold. Results presented as mean ± SD, n > 3 (*$p < 0.0332$, **$p < 0.0021$, ***$p < 0.0002$, ****$p < 0.0001$ *vs* AuNPs 1).

AuNPs	λAbs_{max} (nm)	Abs_{808nm} (a.u.)	Number of Au Atoms per AuNP (x 10^8)	Concentration of AuNPs (x 10^{-9}, mM)	Molar Extinction Coefficient at 808 nm (x 10^{10}, M^{-1}. cm^{-1})
1	550.9 ± 13.5	0.070 ± 0.019	0.94	4.62	1.72 ± 0.26
2	693.3 ± 52.8	0.063 ± 0.006	1.94	2.82	2.23 ± 0.22
3	806.9 ± 142.3 ***	0.086 ± 0.021	1.34	3.69	2.33 ± 0.57
4	645.2 ± 67.1	0.070 ± 0.007	1.39	4.03	1.75 ± 0.17
5	748.1 ± 107.2 **	0.091 ± 0.013	3.12	1.77	5.24 ± 0.92****
6	708.3 ± 120.4	0.088 ± 0.013	2.66	2.35	3.72 ± 0.57****
7	642.4 ± 90.6	0.087 ± 0.029	2.80	1.18	5.91 ± 0.36****
8	603.3 ± 29.6	0.081 ± 0.020	0.55	10.8	0.81 ± 1.88*
9	596.3 ± 17.5	0.081 ± 0.007	1.45	4.39	1.98 ± 0.29
10	626.8 ± 66.2	0.072 ± 0.014	1.25	5.10	1.41 ± 0.29
11	614.4 ± 79.1	0.100 ± 0.022	0.93	6.06	1.66 ± 0.35

(AuNPs 2, 3 and 7) was assessed *in vitro* using the same cell lines (HaCat, MCF-7, HCT-116 and A375). Based on the results from the preliminary *in vitro* safety assessment, 250 μM of gold was the selected concentration for the *in vitro* efficacy assessment. For this, the four cell lines were independently incubated with AuNPs 2, 3 and 7 at 250 μM of gold for 4 h and after this period, the AuNPs-containing medium was replaced with fresh medium and the cells were irradiated, for 5 min, at an irradiance of 7.96 W/cm^2, with a laser emitting at 808 mm. Results are presented in Fig. 8. All nanoformulations except for AuNPs 2 in MCF-7 cells significantly reduced cell viability upon being activated by laser, when compared to the viability of cells incubated with the respective non-activated AuNP formulation. For the same cancer cell lines, only AuNPs 7 reduced cell viability below 70 % in all cell lines upon laser activation: 58.6 % ± 6.6, for MCF-7; 38.5 % ± 7.8, for HCT-116; and 50.6 % ± 9.2, for A375. So, taking these results into account, AuNPs 7 were considered the most effective in reducing the viability of cancer cell lines at 250 μM of gold, upon laser activation.

Besides being effective in reducing the cell viability of cancer cell lines, it is important to mention that the AuNPs, upon activation, did not reduce the viability of human keratinocyte cell line below 70 %. Looking at the results in Fig. 8 for HaCat cells, none of the nanoformulations under study reduced viability below the defined threshold upon activation: 100.9 % ± 6.9 for AuNPs 2 (AuNPs 2 + Laser); 97.5 % ± 6.6 for AuNPs 3 (AuNPs 3 + Laser); and 70.5 % ± 8.3 for AuNPs 7 (AuNPs 7 + Laser), the most effective nanoformulation in the cancer cell lines tested.

3.7. Morphological and elemental characterization of best-performing AuNPs

The best-performing AuNPs (2, 3 and 7) were selected for further analysis, and in order to confirm their AuNP their purity, XRD was performed. The resulting diffractograms are shown in Fig. 9, and it is to note in the diffractograms of AuNPs 2, 3 and 7 the presence of Bragg reflections with 38, 44, 64 and 77 2θ values, correspondent to the (111), (200), (220) and (311) of face center cubic (fcc) lattice for gold [31,32] Moreover, the AuNPs 2, 3 and 7' diffractograms match the simulated AuNPs, and as no other 2θ values were seen, these diffractograms indicate that these are infact AuNPs, of pure nature.

Amongst the three best-performing AuNPs, AuNPs 7 was the most promising, and thus selected for further morphological characterization by STEM, and results are shown in Fig. 10. As observed by the SEM images, AuNPs 7 morphology resemble a nanoflower-like shape.

EDS analysis was also carried out (Fig. 10C), in which it has been detected majority Au, as expected for this pure nanomaterial. Carbon and oxygen were residually detected by EDS, and both elements come from the formvar carbon grid or residuals from the chemical synthesis

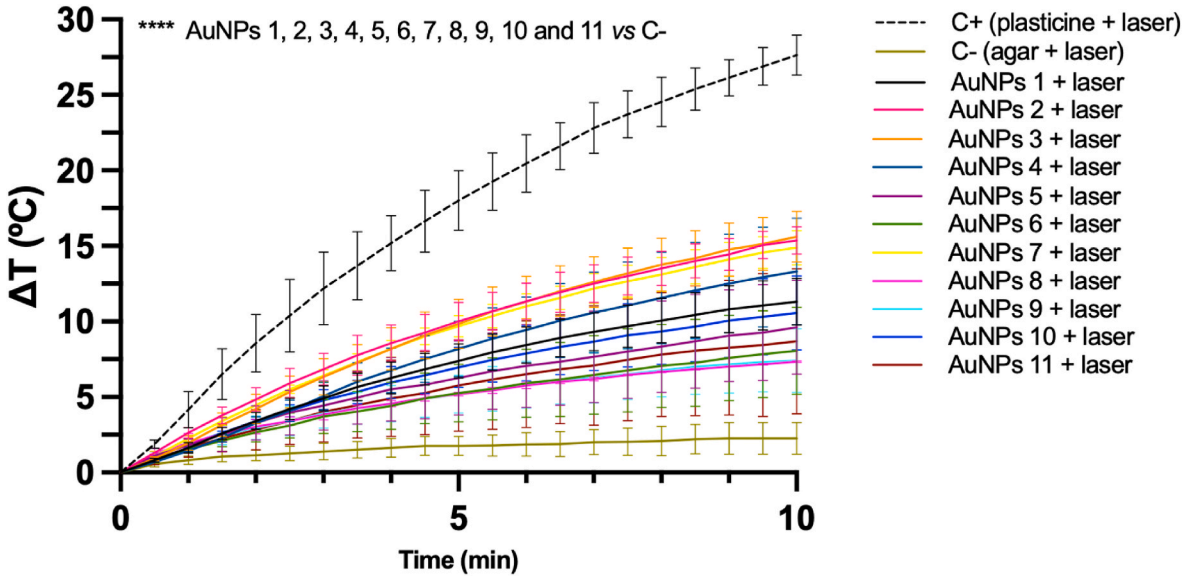

Fig. 3. Temperature increment (°C) of the eleven (1-11) irradiated AuNP formulations as a function of irradiation time by a NIR laser (808 nm, 5.6 W/cm^2), every 30 s up to 10 min. The nanoformulations were incorporated into agar phantoms at 125 μM of gold. The negative control (C-) is agar irradiated by the NIR laser and the positive control (C+) is black plasticine sphere irradiated by the NIR laser. Results are presented as mean ± SD, n = 3 (****$p < 0.0001$ *vs* C-). (For interpretation of the references to color in this figure legend, the reader is referred to the Web version of this article.)

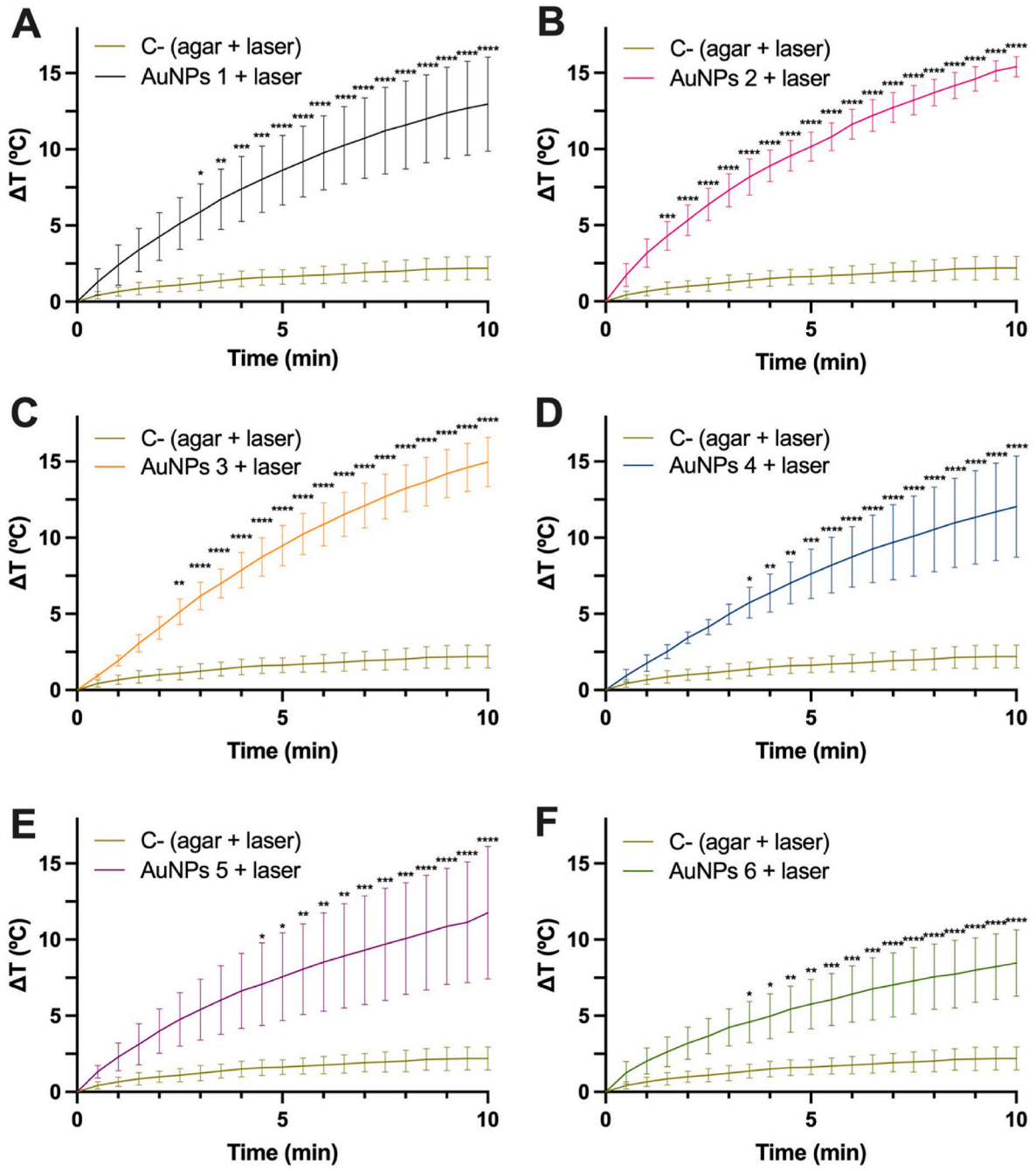

Fig. 4. Temperature increment (°C) of the different irradiated AuNPs' formulations (1–6, A-F, respectively) in function of irradiation time by a NIR laser (808 nm, 5.6 W/cm^2), every 30 s up to 10 min. The nanoformulations were incorporated into agar phantoms at 125 μM of gold. Negative control (C-) is agar irradiated by NIR laser. Results are presented as mean ± SD, (not significative, *ns*, *$p < 0.0332$, **$p < 0.0021$, ***$p < 0.0002$, ****$p < 0.0001$ *vs* C-).
Fig. 4 (cont.). Temperature increment (°C) of the different irradiated AuNPs' formulations (7–11, G-K, respectively) in function of irradiation time by a NIR laser (808 nm, 5.6 W/cm^2), every 30 s up to 10 min. The nanoformulations were incorporated into agar phantoms at 125 μM of gold. Negative control (C-) is agar irradiated by NIR laser. Results are presented as mean ± SD, n = 3 (not significative, *ns*, *$p < 0.0332$, **$p < 0.0021$, ***$p < 0.0002$, ****$p < 0.0001$ *vs* C-). (For interpretation of the references to color in this figure legend, the reader is referred to the Web version of this article.)

[33,34]. No further impurities were detected. Atomic resolution high angle annular dark-field imaging (HAADF-STEM) was used to investigate an individual particle, and in Fig. 10D, it is clear the presence of structural defects, i.e., twin boundaries, which is a common defect found in Au nanocrystals [35–37]. In Fig. 10E, it can be observed atomic columns, with the visible spots corresponding to Au atoms. No differences in contrast (atomic number differences between Au (Z = 79) and Ag (Z = 47)) were observed within the atoms observed, proving that even at the atomic level, no Ag could be detected. The lattice spacings were also measured and the value of 2.35 Å perfectly matches to the {111} lattice planes of the face-centered cubic (FCC) structure of Au. A lattice spacing of 4.08 Å was also measured, corresponding to the (100) plane of Au. Observed along the $[\bar{1}01]$ zone axis, it is clear from the Fast Fourier Transformation (FFT) pattern in Fig. 10F that the angle between (111) and $(1\bar{1}1)$ is ~70.5°, and between the (111) and (100) is ~125° both consistent with the theoretical value for FCC-Au (JCPDS No. 65–2870).

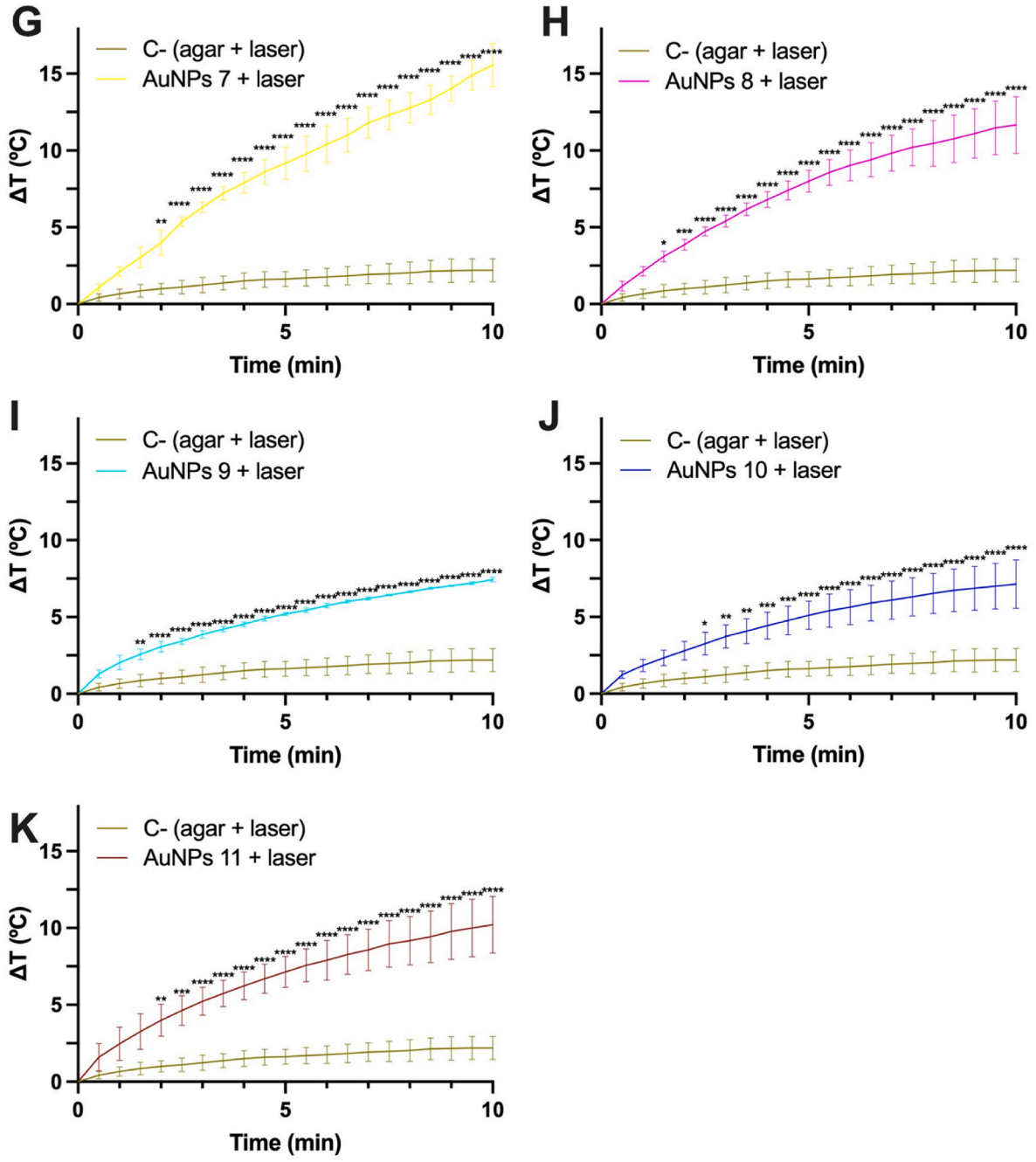

Fig. 4. (*continued*).

4. Discussion

This work focuses on developing an optimized AuNP nanoformulation to be administered *in situ* for PTT, using a NIR laser to activate the AuNPs. A previously developed nanoformulation [8] was used as a starting point (AuNPs 1) and for comparison purposes. The previous AuNPs 1, was formulated using a combination of four solutions, added in the following order: gold (III) chloride trihydride ($HAuCl_4.3H_2O$); silver nitrate ($AgNO_3$); and reducing agents (ascorbic acid and rosmarinic acid). $AgNO_3$ was the first solution to be added to the $HAuCl_4.3H_2O$ solution, and will control the structural growth of the AuNPs, by capping certain facets of the gold seeds and leaving others free for the Au(0) ions to bind. The following agent to be added, ascorbic acid, will reduce the Au(III) present in solution to Au(0), binding together to originate gold seeds. Rosmarinic acid, the last solution to be added in the original order of reagents addition, will reduce the Au(III) left, that were not reduced by ascorbic acid, and the resulting Au(0) ions will bind to the uncapped facets of the gold seeds, originating AuNPs. By changing the addition order of the solutions, and or by removing the $AgNO_3$ solution from the nanoformulations, ten different and new AuNPs' formulations were produced (i.e., AuNPs 2–11). $AgNO_3$ was omitted from formulations AuNPs 2, 4, 8, 9, 10 and 11 as very low volume of $AgNO_3$ solution is used in AuNPs 1, 3, 5, 6 and 7 ($\leq$10 μL). A set of characteristics, that will be discussed below, were defined as target for the selection of the final AuNPs: non-toxic negatively charged AuNPs with an average mean size of around 200 nm and PdI <0.4; Abs_{max} in the NIR (780–3000 nm); homogeneous morphology amongst the nanoformulation; thermal activation with a temperature increase of 6 °C following 3 min of irradiation with the NIR laser. Thus, by changing the order of solution addition, eleven AuNPs' formulations were produced,

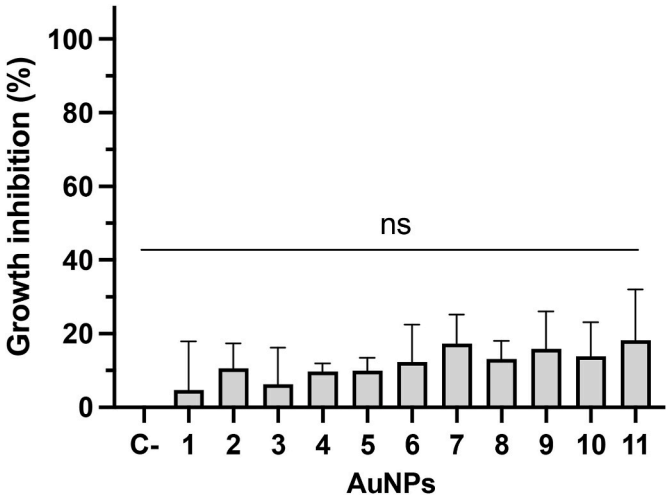

Fig. 5. Growth inhibition (%) of *Saccharomyces kudriavzevii* over a 6 h incubation with the eleven AuNPs' formulations (1-11) at 125 μM of gold. Mean ± SD, n = 9 (not significative, *ns*, *vs* negative control, C-).

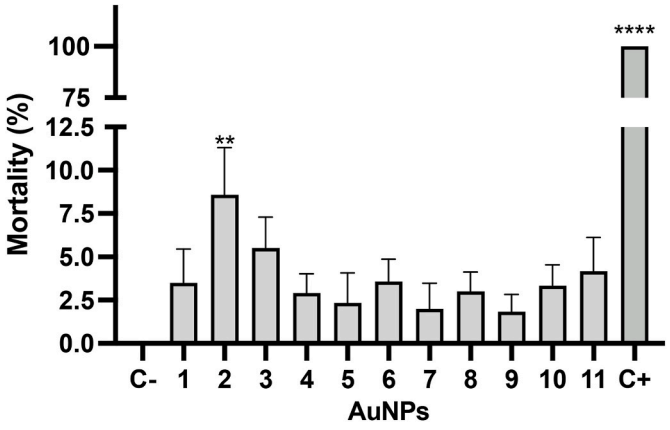

Fig. 6. Mortality (%) of *Artemia salina* incubated, for 24 h, with artificial seawater (negative control, C-), the eleven different AuNPs' formulations (1-11) at 125 μM of gold, and 10 % DMSO (positive control, C+). Mean ± SD, n = 12 (**$p < 0.0021$, ****$p < 0.0001$ *vs* negative control).

with different colorings, physicochemical and optical properties, and different morphologies. Morphology and physicochemical properties (i.e., mean size and PdI) deeply influence optical properties and thus can tune SPR band and the activation potential by a NIR laser [38–42]. Macroscopically the colloidal solutions of the eleven AuNPs presented colours that ranged from burgundies, magentas and blues, which differed between them. The observed change in coloration between nanoformulations was the first indicator that changing the order of addition of solutions had given rise to different AuNPs.

Differences between the colorations of colloidal AuNPs suspensions are usually translated by changes in the mean size of the AuNPs. This was the case for the eleven AuNPs' formulations prepared in this work as all nanoformulations differed in mean size between them. In fact, all nanoformulations, when compared to AuNPs 1, presented higher mean sizes, except for AuNPs 8 and 11. In the present work, the nanoformulations developed are intended to be administered to the tumor *in situ* and get retained at the site of injection. For this, the AuNPs should present a mean size of around 200 nm, as nanoparticles with smaller sizes can reach into blood vessels thus being distributed throughout the body, and into healthy organs and tissues [8,9,43,44]. Taking this into consideration, AuNPs 2 (184 nm), 3 (163 nm), 4 (165 nm), 5 (216 nm), 6 (205 nm), 7 (164 nm), and 9 (167 nm) fit this criteria.

Another important characteristic regarding nanoparticles in colloid suspensions is the size distribution, represented by the PdI. A colloid suspension of AuNPs is desired to present a homogenous distribution of particle size, as this allows better predictability of the nanoformulations' optical (i.e., laser absorption and light-to-heat conversion) and biological (i.e., safety, internalization, biodistribution, etc.) behaviours. Moreover, a monodisperse population of AuNPs also promotes physicochemical stability and increased biocompatibility [45]. PdI varies between 0 (very homogenous and monodisperse) and 1 (very heterogenous and polydisperse), and according to the literature, colloidal suspensions of nanoparticles with PdI's below 0.4 are still considered homogenous [4,9,46–49]. This was the case for all eleven AuNPs and thus all nanoformulations were deemed monodisperse and uniform in size, according to DLS.

Surface charge, evaluated by the determination of the zeta potential, can be positive, neutral or negative. Positively charged nanoparticles are usually associated with higher cytotoxicity [50–52]. Neutral and negatively-charged AuNPs were preferred, as they are less associated with cytotoxicity, agglomeration and reduced organ accumulation in clearance and excretion organs (i.e., liver and kidneys), thus presenting less harmful effects [51–53]. The eleven AuNPs' formulations herein developed presented negative charge, ranging from −22.7 mV, for AuNPs 6, to −30.4 mV, for AuNPs 5. Thus, all AuNPs fulfilled the surface charge requirement (i.e., negatively charged).

Regarding their morphology, overall all AuNPs presented variations of nanoflower-like morphologies depending on the order of addition of the reagents. When the reducing reagents were added at the end of the synthesis, regardless if $AgNO_3$ was included or not, different nanoparticles populations with different mean sizes and morphologies were seen. This may be due to the fact that the reducing agent is dispersed heterogeneously, even under stirring, in the gold salt solution, reducing gold at different strengths throughout the synthesis process, and consequently originating different populations. This was the case for AuNPs 1 (with $AgNO_3$) and AuNPs 2 (without $AgNO_3$), which presented two other populations (planar and quasi-spherical morphologies) of NPs besides a population with nanoflower morphology, as previously described. It is to note that the AuNPs in which the reducing agents were added at the end of the synthesis process (AuNPs 1, 2, 3, 5, 6 and 7), AuNPs present a nanoflower morphology with sharper edges, resembling nanoflowers formed from the compact agglomeration of the other structures seen in AuNP 1 and 2. On the contrary, AuNPs in which the reducing agents were added first, before the contact with the gold salt, (AuNPs 4, 8, 9, 10 and 11), AuNPs presented more compact nanoflowers, that were less branched and without sharp edges, almost quasi-spherical. The difference in the size and sharpness of the branches of the nanoflowers observed when the reducing agents were added before or after the contact with the gold salt can be explained by the rate of dilution of such agents. It has been described that sharper and more branched nanoflowers are formed when there is a heavy dilution of the reducing agents, promoting the reduction and stabilization atom by atom of the nanoflower being formed [54]. This can explain why when the reducing agents were added after the gold salt addition (AuNPs 1, 2, 3, 5, 6 and 7), and thus the reducing agents are highly diluted, the originated particles exhibited sharp and very branched nanoflower morphologies. When the reducing agents were added prior to the gold salt solution (AuNPs 4, 8, 9, 10 and 11), reduction and stabilization occurred more abruptly, as the reducing agents were not diluted in the beginning of the gold salt addition, and thus more compact and less branched nanoflowers were produced. Besides the AuNPs with nanoflower morphology, it is possible to identidy the presence of AuNPs of smaller sizes in AuNPs 1 and 2. Interestingly, the nanoflowers that can be seen resemble the orderly and controlled agglomeration of these smaller AuNPs. This can possibly be explained by the typical formation of AuNPs, including the nucleation and growth of the particles [55,56]. As previously discussed, the first step in the production of AuNPs is the reduction of Au(III) in Au(0), that will stick together and form small gold

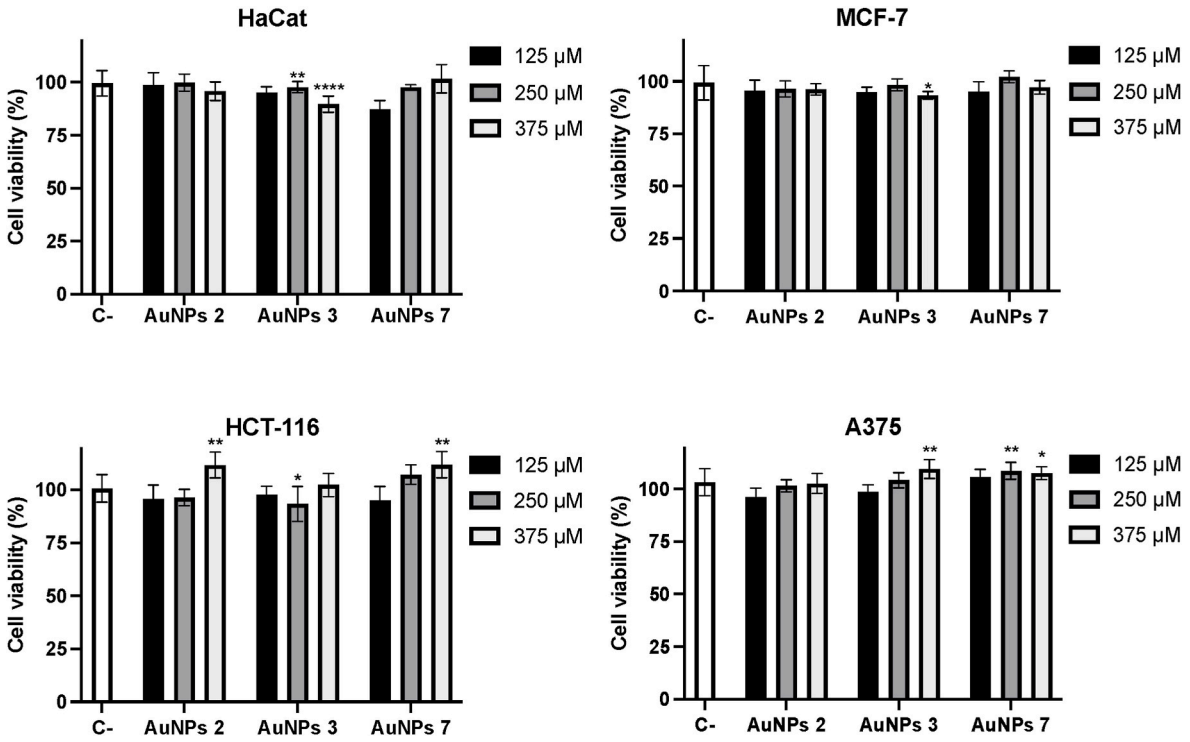

Fig. 7. Cell viability of HaCat, MCF-7, HCT-116 and A375 cell lines after an incubation period of 24 h with the three different AuNPs' formulations (AuNPs 2, AuNPs 3 and AuNPs 7) at three different concentrations of gold: untreated, white columns; 125 μM, black columns; 250 μM, dark grey columns; and 375 μM, light grey columns. Results are presented as mean ± SD, n = 6, (*$p < 0.0332$, **$p < 0.0021$, ****$p < 0.0001$ *vs* untreated cells, C-).

seeds, comprising AuNPs of smaller sizes, possibly the ones seen in AuNPs 1 and 2. After, these gold seeds will agglomerate in a controlled and ordain manner, leading to AuNPs growth, forming the AuNPs nanoflowers of larger size, such as the ones that can be seen in all micrographs, but specially in AuNPs 1–7. The other AuNPs, AuNPs 8–11, might be formed through the same nucleation and growth (*i.e.,* aggregation) processes; however, these aggregates suffer coalescence, compacting the aggregates thus forming more cohesive AuNPs [55,56].

As mentioned, the nanoformulations developed in this work are intended for PTT of localized tumors (i.e., melanoma, breast, head and neck cancer), through the activation by a NIR laser, emitting at 808 nm. Upon being irradiated, the conduction band electrons of the AuNP oscillate in a synchronized manner, resulting in light's scattering or absorption, and when the latter occurs, light is converted into heat [57,58]. The oscillation of the electrons, and thus the rate of light-to-heat conversion, reaches its maximum potential at a specific frequency (SPR) which usually coincides with the maximum absorbance peak (λAbs_{max}) [58–60]. Although, as mentioned, conversion of light into heat is maximized at the λAbs_{max}, corresponding to the peak of SPR, AuNPs are able to convert radiation outside of their λAbs_{max} into heat, as long as the AuNPs absorb radiation in those wavelengths as part of their SPR band. Ideally, as the laser used in this work to photoactivate the AuNPs emits at 808 nm, the SPR band of the AuNPs formulations should be at or very close to 808 nm. Taking into account the λAbs_{max} of the eleven AuNPs prepared in this work, AuNPs 2, 3, 4, 5, 6, and 7 presented SPRs in the NIR wavelengths (780–3000 nm), and AuNPs 3 presented SPR peak close to 808 nm. When comparing to AuNPs 1, the standard nanoformulation, AuNPs 3 and 5 presented significantly higher SPR peaks. Considering Abs at 808 nm (Abs_{808nm}), AuNPs 2 and AuNPs 11 presented the lowest and highest absorption, respectively. Nevertheless among all AuNPs no statistically significant differences in terms of Abs_{808nm} were observed when compared to AuNPs 1.

The efficacy of PTT is dependent on the light-to-heat conversion. To evaluate the *in vitro* thermal activation of the eleven AuNP formulations, agar phantoms containing the AuNPs in a centered well, at a concentration of 125 μM of gold, were prepared and irradiated with the NIR laser for 10 min. Temperature was recorded every 30 s and the temperature differentials were plotted as function of time. All nanoformulations were similar in terms of trace over time, with similar temperature differentials, and all eleven AuNP formulations presented a significant overall higher temperature differential in comparison to the negative control (agar + laser). As previously mentioned the AuNPs 11 formulation was the one that presented the highest absorption value at 808 nm, but this was not translated into a higher degree of significance of temperature increase when compared to the negative control. In fact, this nanoformulation (AuNPs 11) was the one that presented the lowest number of time points with significantly different temperature differentials compared to AuNPs 1, with zero time points with significantly different temperature differentials, while AuNPs 2, 3 and 7 were the nanoformulations that presented the highest number of time points with statistical significantly different temperature differentials. This result is of great interest as AuNPs 3 was the nanoformulation that presented the SPR peak closest to the wavelength at which the laser emits, at 808 nm, and as mentioned, the SPR peak represents the wavelength at which the light into heat conversion is more efficient. Thus, AuNP 2, 3 and 7 satisfied the defined optical properties requirements: presenting SPR peak in the NIR and being able to efficiently convert light into heat by originating a significant temperature increase throughout the 10 min of laser irradiation, increasing ≥ 6 °C following a 3 min of irradiation.

Green synthesis of AuNPs using secondary metabolites, such as rosmarinic and L-ascorbic acids, have attracted attention in order to replace the toxic reagents used in the conventional methods for AuNPs preparations, that are considered hazardous to human health and enviroment [61]. Due to this, many several plant secondary metabolites are explored for their possible application in the green synthesis of metallic nanoparticles (i.e., AuNPs and silver nanoparticles, AgNPs), such as apigenin, curcumin, gallic acid, rosmarinic acid and L-ascorbic acid [62–66]. Still, and the same for the synthetic compounds, it is always important to ensure that AuNPs prepared by green synthesis methods are safe, both *in vitro* and *in vivo*.

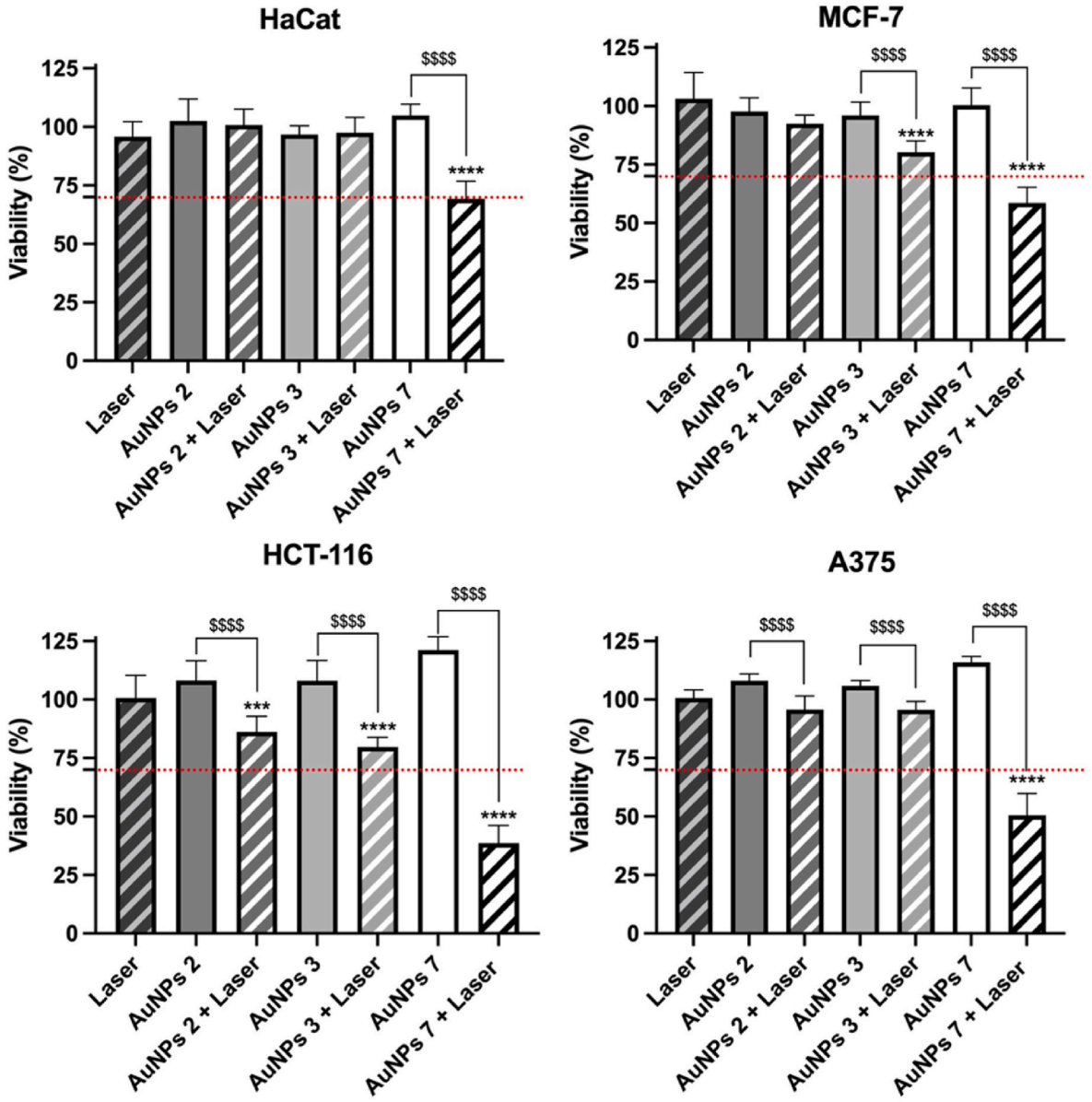

Fig. 8. Cell viability of HaCat, MCF-7, HCT-116 and A375 cell lines after an incubation period of 4 h with the three different AuNPs (AuNPs 2, AuNPs 3 and AuNPs 7) at 250 μM of gold, activated by laser (7.96 W/cm^2, 5 min) (striped columns) or not activated by laser (full columns). Dotted red line represents a cell viability of 70 %. Results are presented as mean ± SD, n = 6, (***$p < 0.0002$, ****$p < 0.0001$ *vs* untreated cells, not shown; $^{\$\$\$\$}p < 0.0001$ *vs* respective non-activated AuNPs formulation). (For interpretation of the references to color in this figure legend, the reader is referred to the Web version of this article.)

Saccharomyces spp., especially *Saccharomyces cerevisiae* and *Saccharomyces kudriavzevii*, are unicellular eukaryotic organisms commonly used in biological studies, including safety and cytotoxicity assessments of drugs and nanoparticles [7,28,67–70]. Some species of *Saccharomyces* spp. present similar cellular and metabolic pathways to the ones found in mammal cells, with some genes and processes being conserved, or presenting orthologues, in humans [67–69]. With this in mind, safety of the eleven AuNPs was evaluated by analyzing the growth curves of *S. kudriavzevii* in the presence of the nanoformulations. None of the eleven AuNPs presented toxicity in the *S. kudriavzevii* model. Next, *Artemia salina* model was selected to preliminarily assess the safety of the eleven nanoformulations in a multicellular invertebrate method, as this model allows for a quick toxicity determination at a low cost, and has been previously used for the evaluation of potential toxicity of heavy metals and nanoparticles [4,9,70]. For this *in vivo* model, no toxicity was observed for the eleven AuNP formulations except for AuNPs 2 when compared to AuNPs 1. However, the toxicity of AuNPs 2 was still very low (8.6 %, <10 %) when compared to the positive control.

As none of the tested AuNPs raised toxicity concerns in the *S. kudriavevii* and *A. salina* models, the decision of what formulations would be further tested in *in vitro* assessments was based on the results of the *in vitro* thermal activation. As the AuNP that more efficiently converted light into heat were AuNPs 2, 3 and 7, these were the three nanoformulations selected for further testing.

In vitro safety assessments were also performed using a variety of cell lines that included human keratinocytes (HaCat) and cancerous (MCF-7, breast cancer; HCT-116, colon cancer; and A375, melanoma) commercial cell lines. The optimized nanoformulation is intended to preserve cell viability of healthy or cancer cells when not activated by laser irradiation, as was proven by the obtained results. Indeed, after a 24 h incubation period, cell viability of all cell lines remained above 85 % for AuNPs 2, 3 and 7 and at three different gold concentrations (125, 250 and 375 μM).

Although safety is one key concern during the optimization of the

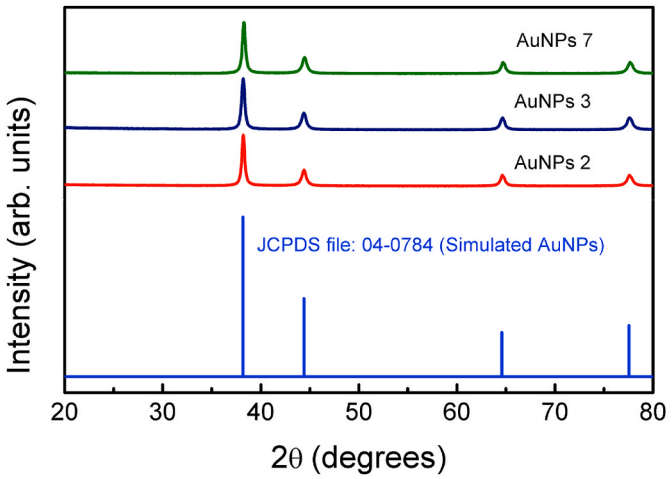

Fig. 9. XRD diffractograms of AuNPs 2 (red), 3 (dark blue) and 7 (green). A diffractogram of simulated AuNPs (light blue) is shown for comparison. (For interpretation of the references to color in this figure legend, the reader is referred to the Web version of this article.)

AuNPs for PTT, it is also important to maximize the photothermal conversion potential of the nanoformulation.

The efficacy of the most promising AuNPs was performed by testing the same cell lines as the ones used in the safety *in vitro* studies. After an incubation period of 4 h, cells in the presence or absence of AuNPs were submitted to a laser activation period of 5 min, by laser irradiation at 808 nm 7.96 W/cm^3. The concentration used was 250 μM since the cell viability was above 90 % for all cell lines. Activated AuNPs 2 was the least effective nanoformulation, resulting in the lowest reduction of cellular viability in all cell lines upon laser activation. This nanoformulation, upon laser irradiation, significantly reduced cell viability in HCT-116 (86 %) and A375 (96 %) cell lines, but not in MCF-7 (92 %), in comparison to non-laser activated AuNPs 2 (108 % for HCT-116, 108 % for A375, and 98 % for MCF-7), while activated AuNPs 3 and 7 significantly reduced cell viability in all cancer cell lines in comparison to the respective non-laser activated AuNPs 3 (80 % *vs* 96 % for MCF-7, 80 % *vs* 108 % for HCT-116, and 96 % *vs* 106 % for A375; activated *vs* non-laser activated AuNPs 3) and 7 (59 % *vs* 100 % for MCF-7, 39 % *vs* 121 % for HCT-116, and 51 % *vs* 116 % for A375; activated *vs* non-laser activated AuNPs 7). AuNPs 7 was the only nanoformulation that significantly reduced cell viability below 70 % in all cancer cell lines tested, indicating that this is the most promising one for PTT. Furthermore, none of the AuNP formulations reduced HaCat cell viability upon laser irradiation, indicating that the activated AuNPs 2, 3 and 7 are safe for healthy cells (i.e., HaCat).

Although AuNPs 2, 3 and 7 presented similar thermal activation profiles to each other, the *in vitro* efficacy studies showed some differences that can be explained by the differences in their optical properties. For once, although the differences were not significative in comparison to AuNPs 1 (standard formulation), AuNPs 7 (0.087) is the AuNP formulation with the highest Abs_{808nm} when compared to AuNPs 2

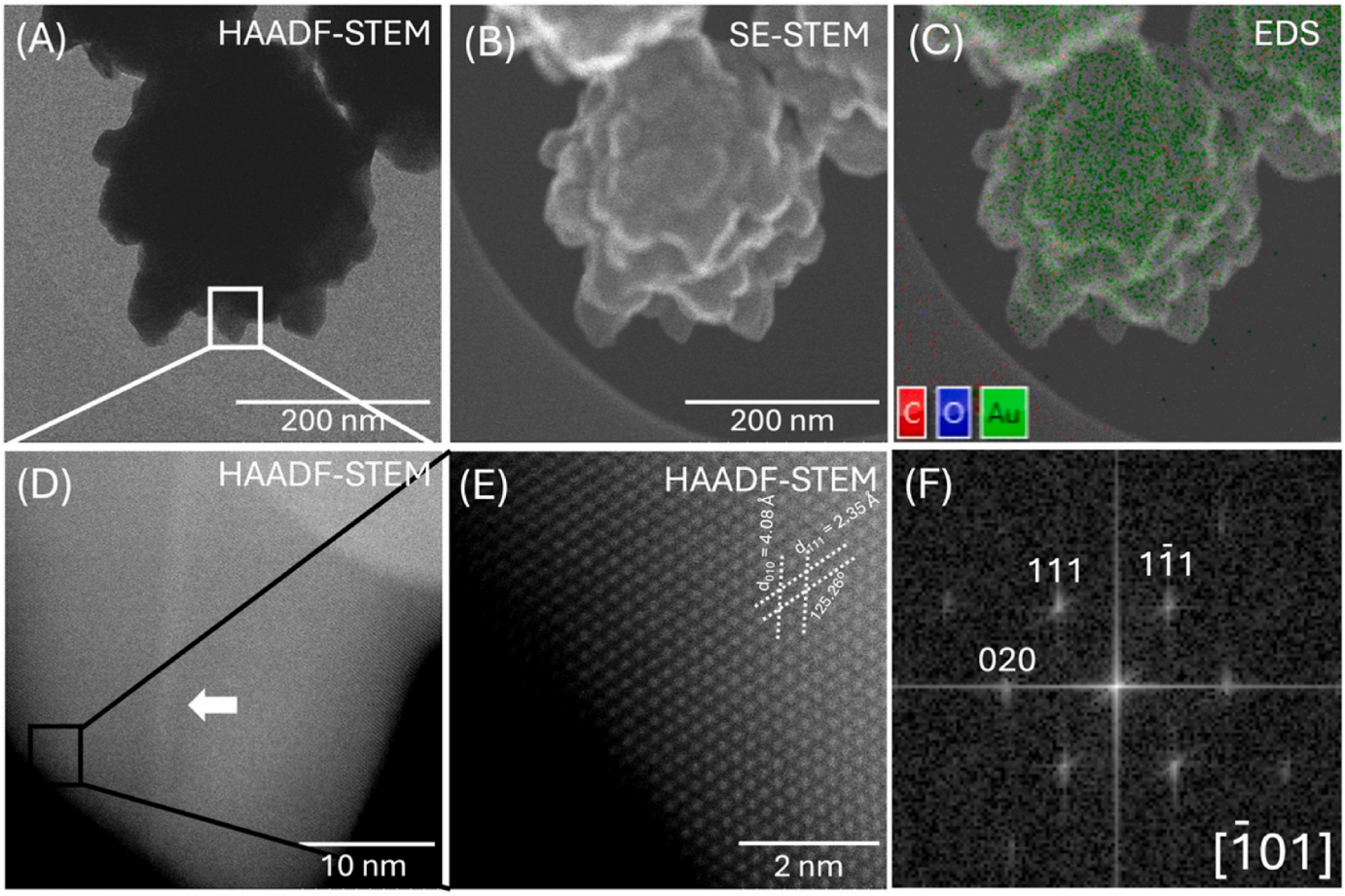

Fig. 10. (A) HAADF-STEM image of an individual AuNP from condition 7 together with the secondary electron (SE) image that was obtained simultaneously. (C) EDS analysis of the same particle demonstrating that it is Au-rich, without any impurities detected. (D) Magnified HAADF-STEM images of an individual branch, where it is visible the presence of a twin boundary (white arrow). (E) Atomic-resolution HAADF-STEM image of the area indicated in (D). (F) FFT image of the area analyzed in (E).

(0.063) and 3 (0.086), at the same concentration of gold. However, among these nanoformulations, AuNPs 7 was the one that presented the highest molar extinction coefficient at 808 nm, the wavelength at which the laser emits to activate the AuNPs. The molar extinction coefficient of AuNPs at a certain wavelength represents how strongly AuNPs absorb radiation at that specific wavelength, and the molar extinction wavelengths for AuNPs 2, 3 and 7 were 2.23×10^{10}, 2.33×10^{10} and 5.91×10^{10} M^{-1} cm^{-1}, respectively. Thus, when the AuNPs 7-containing cell wells were irradiated at 808 nm during the preliminary *in vitro* efficacy assays, this was the AuNPs formulation that greatly absorbed the laser radiation, and consequently, was the utmost activated nanoformulation.

Taking all results into account, the synthesis of AuNPs 7 seems to be the best nanoformulation based on the order of reagents addition as follows: $HAuCl_4.3H_2O$; L-ascorbic acid; $AgNO_3$; and rosmarinic acid. All reagents seem to have unique roles in this AuNPs synthesis method. We propose that L-ascorbic acid should be the primary reducing agent of $HAuCl_4.3H_2O$, reducing Au(III) to A(0) ions, that will stick together to form the AuNP nuclei, originating gold seeds [71–73]. Furthermore, the originated gold seeds are thought to be capped by L-ascorbic acid's oxidized form, dehydroascorbic acid, as previously described for other methods of AuNP preparation [74]. Thus, for AuNPs 7, as well as for other orders of additions in which L-ascorbic acid was the primary reducing agent (i.e., AuNPs 1, 2, 6 and 11), this reducing agent is thought to have a double action as reducing and capping agent. The third reagent to be added in the preparation of AuNPs 7 is $AgNO_3$. Although $AgNO_3$ is present in very low concentrations during the synthesis (1 mM, $\leq$10 μL), it might present an important role for the desired characteristics to be attained, as its omission results in different properties (AuNPs 2). One of the main characteristics to change when the same order or reagents addition was used but $AgNO_3$ was omitted was morphology. By comparing the morphology of AuNPs 2 and AuNPs 7, it is to note that the presence of $AgNO_3$ (AuNPs 7) resulted in isolated and uniform AuNPs with nanoflower morphology with more pronounced and sharper branches, while the omission of $AgNO_3$ originated AuNPs with different populations, while nanoflower-like morphologies were present. In the last one, these were less branched and the branches were more dull. This might indicate that, $AgNO_3$ should preferentially bind to certain facets of the gold seeds originated by L-ascorbic acids' reduction of $HAuCl_4.3H_2O$ [75,76]. This binding will promote the growth of the uncovered/unbound surfaces of the nanocrystal, forming the sharp nanoflower branches, and thus $AgNO_3$ might act in directing the branches' growth [71,75]. Moreover, $AgNO_3$ can react with the Cl^- ions from the not-reduced $HAuCl_4.3H_2O$ still present in the synthesis, making it more available to be reduced by the next reducing agent, rosmarinic acid. This reducing agent is the last reagent added in AuNPs 7 synthesis, and as said, will reduce the leftover $HAuCl_4.3H_2O$, again from Au(III) to A(0) ions. These sticky ions seem to bind to the surface of the gold seed nanocrystal available.

5. Conclusion

The current work explored the methodology of AuNPs synthesis and how changing the order of addition of the reducing and stabilizing reagents used influences the physicochemical and optical properties of the product, and consequently the efficacy for a potential application in AuNPs-mediated PTT. Results showed that the main differences were in terms of surface morphology, especially dependent on when the reducing agents were added (if before or after the contact with the gold salt), but also presented changes in optical properties, particularly in the AuNPs' molar extinction coefficient and thermal activation profiles. The highest molar extinction coefficients at 808 nm, translating how strongly AuNPs absorb light at this wavelength, were obtained when one reducing agent (regardless of rosmarinic acid or ascorbic acid) was added immediately after contact with the gold salt, and followed by the addition of $AgNO_3$. Moreover, the strongest thermal activation profiles were achieved when the gold salt was the first to be added, followed by ascorbic acid or $AgNO_3$. The AuNPs formulations with the strongest thermal activation profiles were shown to be safe *in vitro*, using different cell lines, and *in vivo*, using *Saccharomyces kudriavzevii* and *Artemia salina* models. Furthermore, the efficacy of these nanoformulations was shown *in vitro*, upon laser activation at 808 nm, with the most efficient nanoformulation (AuNPs 7) resulting in a cell viability decrease of $\geq$45 % in all cancer cell lines tested.

Additionally, these results also corroborate that the order of reagent addition is a crucial step in the optimization of AuNPs synthesis as this will affect the overall properties, and consequently change the biocompatibility and photothermal conversion ability, further impacting the efficacy of AuNPs-mediated PTT.

Funding

Fundação para a Ciência e Tecnologia (FCT) through projects UIDB/00645/2020 (https://doi.org/10.54499/UIDB/00645/2020), UIDP/00645/2020 (https://doi.org/10.54499/UIDP/00645/2020), UIDB/04138/2020, UIDP/04138/2020 and PTDC/QUI-QIN/0586/2020, but also the PhD fellowship SFRH/BD/05377/2021.

CRediT authorship contribution statement

Mariana Neves Amaral: Writing – original draft, Methodology, Investigation, Formal analysis, Data curation. **Daniela Nunes:** Writing – review & editing, Methodology, Investigation, Formal analysis. **Elvira Fortunato:** Funding acquisition. **Rodrigo Martins:** Funding acquisition. **Carla Rodrigues:** Writing – review & editing, Methodology, Investigation. **Pedro Faísca:** Supervision. **Hugo Alexandre Ferreira:** Writing – review & editing, Supervision. **João M.P. Coelho:** Writing – review & editing, Methodology, Investigation, Funding acquisition, Conceptualization. **M. Manuela Gaspar:** Writing – review & editing, Project administration, Methodology, Investigation, Formal analysis. **Catarina Pinto Reis:** Writing – review & editing, Project administration, Methodology, Investigation, Funding acquisition, Formal analysis, Conceptualization.

Declaration of competing interest

The authors declare that they have no known competing financial interests or personal relationships that could have appeared to influence the work reported in this paper.

Data availability

Data will be made available on request.

Acknowledgements

The authors would like to acknowledge the Laboratório de Análises/REQUIMTE/LAQV for the acquisition of the ICP-OES data and Maria Leonor Matias for her support in XRD.

Appendix A. Supplementary data

Supplementary data to this article can be found online at https://doi.org/10.1016/j.jddst.2024.106215.

References

[1] S. Nomura, Y. Morimoto, H. Tsujimoto, M. Arake, M. Harada, D. Saitoh, I. Hara, E. Ozeki, A. Satoh, E. Takayama, K. Hase, Y. Kishi, H. Ueno, Highly reliable, targeted photothermal cancer therapy combined with thermal dosimetry using a near-infrared absorbent, Sci. Rep. 10 (2020) 9765, https://doi.org/10.1038/s41598-020-66646-x.

[2] G. Gao, X. Sun, G. Liang, Nanoagent-promoted mild-temperature photothermal therapy for cancer treatment, Adv. Funct. Mater. 31 (2021) 2100738, https://doi.org/10.1002/adfm.202100738.
[3] J. Lopes, C.M.P. Rodrigues, M.M. Gaspar, C.P. Reis, How to treat melanoma? The current status of innovative nanotechnological strategies and the role of minimally invasive approaches like PTT and PDT, Pharmaceutics 14 (2022) 1817, https://doi.org/10.3390/pharmaceutics14091817.
[4] J. Lopes, T. Ferreira-Gonçalves, L. Ascensão, A.S. Viana, L. Carvalho, J. Catarino, P. Faísca, A. Oliva, D.P.C. de Barros, C.M.P. Rodrigues, M.M. Gaspar, C.P. Reis, Safety of gold nanoparticles: from in vitro to in vivo testing array checklist, Pharmaceutics 15 (2023) 1120, https://doi.org/10.3390/pharmaceutics15041120.
[5] M.N. Amaral, P. Faísca, H.A. Ferreira, M.M. Gaspar, C.P. Reis, Current insights and progress in the clinical management of head and neck cancer, Cancers 14 (2022) 6079, https://doi.org/10.3390/cancers14246079.
[6] J. Lopes, T. Ferreira-Gonçalves, I.V. Figueiredo, C.M.P. Rodrigues, H. Ferreira, D. Ferreira, A.S. Viana, P. Faísca, M.M. Gaspar, J.M.P. Coelho, C.O. Silva, C.P. Reis, Proof-of-Concept study of multifunctional hybrid nanoparticle system combined with NIR laser irradiation for the treatment of melanoma, Biomolecules 11 (2021) 511, https://doi.org/10.3390/biom11040511.
[7] J. Lopes, J.M.P. Coelho, P.M.C. Vieira, A.S. Viana, M.M. Gaspar, C. Reis, Preliminary assays towards melanoma cells using phototherapy with gold-based nanomaterials, Nanomaterials 10 (2020) 1536, https://doi.org/10.3390/nano10081536.
[8] M. Amaral, A.J. Charmier, R.A. Afonso, J. Catarino, P. Faísca, L. Carvalho, L. Ascensão, J.M.P. Coelho, M.M. Gaspar, C.P. Reis, Gold-based nanoplataform for the treatment of anaplastic thyroid carcinoma: a step forward, Cancers 13 (2021) 1242, https://doi.org/10.3390/cancers13061242.
[9] T. Ferreira-Gonçalves, M.M. Gaspar, J.M.P. Coelho, V. Marques, A.S. Viana, L. Ascensão, L. Carvalho, C.M.P. Rodrigues, H.A. Ferreira, D. Ferreira, C.P. Reis, The role of rosmarinic acid on the bioproduction of gold nanoparticles as part of a photothermal approach for breast cancer treatment, Biomolecules 12 (2022) 71, https://doi.org/10.3390/biom12010071.
[10] E. Costa, T. Ferreira-Gonçalves, M. Cardoso, J.M.P. Coelho, M.M. Gaspar, P. Faísca, L. Ascensão, A.S. Cabrita, C.P. Reis, I.V. Figueiredo, A step forward in breast cancer research: from a natural-like experimental model to a preliminary photothermal approach, Int. J. Mol. Sci. 21 (2020) 9681, https://doi.org/10.3390/ijms21249681.
[11] C.O. Silva, P. Rijo, J. Molpeceres, L. Ascensão, A. Roberto, A.S. Fernandes, R. Gomes, J.M. Pinto Coelho, A. Gabriel, P. Vieira, C.P. Reis, Bioproduction of gold nanoparticles for photothermal therapy, Ther. Deliv. 7 (2016) 287–304, https://doi.org/10.4155/tde-2015-0011.
[12] C.O. Silva, S.B. Petersen, C.P. Reis, P. Rijo, J. Molpeceres, A.S. Fernandes, O. Gonçalves, A.C. Gomes, I. Correia, H. Vorum, M.T. Neves-Petersen, EGF functionalized polymer-coated gold nanoparticles promote EGF photostability and EGFR internalization for photothermal therapy, PLoS One 11 (2016) e0165419, https://doi.org/10.1371/journal.pone.0165419.
[13] M. Amaral, N. Cruz, A. Rosa, B. Nogueira, D. Costa, F. Santos, M. Brazão, P. Policarpo, R. Mateus, Y. Kobozev, C.P. Reis, An update of advanced nanoplatforms for Glioblastoma Multiforme Management, EXCLI J 20 (2021) 1544–1570, https://doi.org/10.17179/excli2021-4393.
[14] J.O. Pinho, J. Lopes, M. Albino, C. Reis, M. Matias, M.M. Gaspar, Advances in nanotechnology-related strategies against melanoma, in: R.B.T.-M.D. M, N. de Oliveira (Eds.), Mitochondrial Dysfunct. Nanotherapeutics, Elsevier, 2021, pp. 385–424, https://doi.org/10.1016/B978-0-323-85666-9.00009-7.
[15] T. Ferreira-Gonçalves, D. Ferreira, H.A. Ferreira, C.P. Reis, Nanogold-based materials in medicine: from their origins to their future, Nanomedicine 16 (2021) 2695–2723, https://doi.org/10.2217/nnm-2021-0265.
[16] R. Ahmad, J. Fu, N. He, S. Li, Advanced gold nanomaterials for photothermal therapy of cancer, J. Nanosci. Nanotechnol. 16 (2016) 67–80, https://doi.org/10.1166/jnn.2016.10770.
[17] S. Liao, W. Yue, S. Cai, Q. Tang, W. Lu, L. Huang, T. Qi, J. Liao, Improvement of gold nanorods in photothermal therapy: recent progress and perspective, Front. Pharmacol. 12 (2021), https://doi.org/10.3389/fphar.2021.664123.
[18] T. Ferreira-Gonçalves, A. Iglesias-Mejuto, T. Linhares, J.M.P. Coelho, P. Vieira, P. Faísca, J. Catarino, P. Pinto, D. Ferreira, H.A. Ferreira, M.M. Gaspar, L. Durães, C.A. García-González, C.P. Reis, Biological thermal performance of organic and inorganic aerogels as patches for photothermal therapy, Gels 8 (2022) 485, https://doi.org/10.3390/gels8080485.
[19] A. Doughty, A. Hoover, E. Layton, C. Murray, E. Howard, W. Chen, Nanomaterial applications in photothermal therapy for cancer, Materials 12 (2019) 779, https://doi.org/10.3390/ma12050779.
[20] V. Frantellizzi, V. Verrina, C. Raso, M. Pontico, F. Petronella, V. Bertana, A. Ballesio, S.L. Marasso, S. Miglietta, P. Rosa, S. Scibetta, V. Petrozza, M.S. De Feo, G. De Vincentis, A. Calogero, R. Pani, G. Perotto, L. De Sio, 99mTc-labeled keratin gold-nanoparticles in a nephron-like microfluidic chip for photo-thermal therapy applications, Mater. Today Adv. 16 (2022) 100286, https://doi.org/10.1016/j.mtadv.2022.100286.
[21] M. Chirivì, C. Bearzi, P. Rosa, S. Miglietta, F. Petronella, E. De Falco, A. Calogero, R. Pani, V. Petrozza, G. Perotto, R. Rizzi, L. De Sio, Biomimetic keratin-coated gold nanoparticles for photo-thermal therapy in a 3D bioprinted glioblastoma tumor model, Int. J. Mol. Sci. 23 (2022) 9528, https://doi.org/10.3390/ijms23179528.
[22] A. Guglielmelli, P. Rosa, M. Contardi, M. Prato, G. Mangino, S. Miglietta, V. Petrozza, R. Pani, A. Calogero, A. Athanassiou, G. Perotto, L. De Sio, Biomimetic keratin gold nanoparticle-mediated in vitro photothermal therapy on glioblastoma multiforme, Nanomedicine. 16 (2021) 121–138, https://doi.org/10.2217/nnm-2020-0349.
[23] I. Elsayed, X. Huang, M. Elsayed, Selective laser photo-thermal therapy of epithelial carcinoma using anti-EGFR antibody conjugated gold nanoparticles, Cancer Lett. 239 (2006) 129–135, https://doi.org/10.1016/j.canlet.2005.07.035.
[24] S. Lal, S.E. Clare, N.J. Halas, Nanoshell-enabled photothermal cancer therapy: impending clinical impact, Acc. Chem. Res. 41 (2008) 1842–1851, https://doi.org/10.1021/ar800150g.
[25] W. Yang, H. Liang, S. Ma, D. Wang, J. Huang, Gold nanoparticle based photothermal therapy: development and application for effective cancer treatment, Sustain. Mater. Technol. 22 (2019) e00109, https://doi.org/10.1016/j.susmat.2019.e00109.
[26] I. Ojea-Jiménez, N.G. Bastús, V. Puntes, Influence of the sequence of the reagents addition in the citrate-mediated synthesis of gold nanoparticles, J. Phys. Chem. C 115 (2011) 15752–15757, https://doi.org/10.1021/jp2017242.
[27] T. Ferreira-Gonçalves, D. Nunes, E. Fortunato, R. Martins, A.P. de Almeida, L. Carvalho, D. Ferreira, J. Catarino, P. Faísca, H.A. Ferreira, M. Manuela Gaspar, J. M.P. Coelho, C. Pinto Reis, Rational Approach to Design Gold Nanoparticles for Photothermal Therapy: the effect of gold salt on physico-chemical, optical and biological properties, Int. J. Pharm. (2023) 123659, https://doi.org/10.1016/j.ijpharm.2023.123659.
[28] A. Roberto, P.P. Caetano, A high-throughput screening method for general cytotoxicity part I Chemical toxicity, Rev. Lusófona Ciências e Tecnol. Da Saúde. 2 (2005) 95–100.
[29] M. Amaral, A.S. Martins, J. Catarino, R.P.B.M. Faísca, P. Kumar, J. Pinto, R. Pinto, et al., How can biomolecules improve mucoadhesion of oral insulin? A comprehensive insight using ex-vivo, in silico and in vivo models, Biomolecules (2020), https://doi.org/10.3390/biom10050675.
[30] R. Pecoraro, E.M. Scalisi, G. Messina, G. Fragalà, S. Ignoto, A. Salvaggio, M. Zimbone, G. Impellizzeri, M.V. Brundo, Artemia salina : a microcrustacean to assess engineered nanoparticles toxicity, Microsc. Res. Tech. 84 (2021) 531–536, https://doi.org/10.1002/jemt.23609.
[31] M. Singh, R. Kalaivani, S. Manikandan, N. Sangeetha, A.K. Kumaraguru, Facile green synthesis of variable metallic gold nanoparticle using Padina gymnospora, a brown marine macroalga, Appl. Nanosci. 3 (2013) 145–151, https://doi.org/10.1007/s13204-012-0115-7.
[32] S. Krishnamurthy, A. Esterle, N.C. Sharma, S.V. Sahi, Yucca-derived synthesis of gold nanomaterial and their catalytic potential, Nanoscale Res. Lett. 9 (2014) 627, https://doi.org/10.1186/1556-276X-9-627.
[33] W.H. De Jong, M.C. Burger, M.A. Verheijen, R.E. Geertsma, Detection of the presence of gold nanoparticles in organs by transmission electron microscopy, Materials 3 (2010) 4681–4694, https://doi.org/10.3390/ma3094681.
[34] M. Erasmus, O.A. Idris, A.I. Adetunji, E.D. Cason, Biogenic synthesis and characterization of gold nanoparticles using transformed mesophilic Escherichia coli BL21 and thermophilic Thermus thermophilus HB27, Biologia 79 (2024) 2605–2619, https://doi.org/10.1007/s11756-024-01733-2.
[35] C. Fernández-Lodeiro, J. Fernández-Lodeiro, A. Fernández-Lodeiro, S. Nuti, C. Lodeiro, A. LaGrow, I. Pérez-Juste, J. Pérez-Juste, I. Pastoriza-Santos, Synthesis of tuneable gold nanostars: the role of adenosine monophosphate, J. Mater. Chem. C 11 (2023) 12626–12636, https://doi.org/10.1039/D3TC01567J.
[36] W. Li, W. Tong, A. Yadav, E. Bladt, S. Bals, A.M. Funston, J. Etheridge, Shape control beyond the seeds in gold nanoparticles, Chem. Mater. 33 (2021) 9152–9164, https://doi.org/10.1021/acs.chemmater.1c02459.
[37] C.L. Nehl, H. Liao, J.H. Hafner, Optical properties of star-shaped gold nanoparticles, Nano Lett. 6 (2006) 683–688, https://doi.org/10.1021/nl052409y.
[38] X. Zhang, Gold nanoparticles: recent advances in the biomedical applications, Cell Biochem. Biophys. 72 (2015) 771–775, https://doi.org/10.1007/s12013-015-0529-4.
[39] V.K. Pustovalov, L.G. Astafyeva, W. Fritzsche, Optical properties of core–shell gold–silver and silver–gold nanoparticles for near UV and visible radiation wavelengths, Plasmonics 7 (2012) 469–474, https://doi.org/10.1007/s11468-012-9330-z.
[40] X. Huang, M.A. El-Sayed, Gold nanoparticles: optical properties and implementations in cancer diagnosis and photothermal therapy, J. Adv. Res. 1 (2010) 13–28, https://doi.org/10.1016/j.jare.2010.02.002.
[41] V.A. Ogarev, V.M. Rudoi, O.V. Dement'eva, Gold nanoparticles: synthesis, optical properties, and application, Inorg. Mater. Appl. Res. 9 (2018) 134–140, https://doi.org/10.1134/S2075113318010197.
[42] E.S. Kooij, W. Ahmed, C. Hellenthal, H.J.W. Zandvliet, B. Poelsema, From nanorods to nanostars: tuning the optical properties of gold nanoparticles, Colloids Surfaces A Physicochem. Eng. Asp. 413 (2012) 231–238, https://doi.org/10.1016/j.colsurfa.2012.01.041.
[43] K. Maruyama, Intracellular targeting delivery of liposomal drugs to solid tumors based on EPR effects, Adv. Drug Deliv. Rev. 63 (2011) 161–169, https://doi.org/10.1016/j.addr.2010.09.003.
[44] H. Kobayashi, R. Watanabe, P.L. Choyke, Improving conventional enhanced permeability and retention (EPR) effects; what is the appropriate target? Theranostics 4 (2014) 81–89, https://doi.org/10.7150/thno.7193.
[45] L. Melo, A. Hui, M. Kowal, E. Boateng, Z. Poursorkh, E. Rocheron, J. Wong, A. Christy, E. Grant, Size distributions of gold nanoparticles in solution measured by single-particle mass photometry, J. Phys. Chem. B 125 (2021) 12466–12475, https://doi.org/10.1021/acs.jpcb.1c05557.
[46] H.K. Ardani, C. Imawan, W. Handayani, D. Djuhana, A. Harmoko, V. Fauzia, Enhancement of the stability of silver nanoparticles synthesized using aqueous extract of Diospyros discolor Willd. leaves using polyvinyl alcohol, IOP Conf. Ser.

Mater. Sci. Eng. 188 (2017) 012056, https://doi.org/10.1088/1757-899X/188/1/012056.
[47] A.S. Eissa, Effect of SDS on whey protein polymers. Molecular investigation via dilute solution viscometry and dynamic light scattering, Food Hydrocolloids 87 (2019) 97–100, https://doi.org/10.1016/j.foodhyd.2018.07.046.
[48] A. Fouda, A.M. Eid, E. Guibal, M.F. Hamza, S.E.-D. Hassan, D.H.M. Alkhalifah, D. El-Hossary, Green synthesis of gold nanoparticles by aqueous extract of zingiber officinale: characterization and insight into antimicrobial, antioxidant, and in vitro cytotoxic activities, Appl. Sci. 12 (2022) 12879, https://doi.org/10.3390/app122412879.
[49] D.S. Salem, M.A. Sliem, M. El-Sesy, S.A. Shouman, Y. Badr, Improved chemo-photothermal therapy of hepatocellular carcinoma using chitosan-coated gold nanoparticles, J. Photochem. Photobiol. B Biol. 182 (2018) 92–99, https://doi.org/10.1016/j.jphotobiol.2018.03.024.
[50] E. Fröhlich, The role of surface charge in cellular uptake and cytotoxicity of medical nanoparticles, Int. J. Nanomed. (2012) 5577, https://doi.org/10.2147/IJN.S36111.
[51] V. Yagublu, A. Karimova, J. Hajibabazadeh, C. Reissfelder, M. Muradov, S. Bellucci, A. Allahverdiyev, Overview of physicochemical properties of nanoparticles as drug carriers for targeted cancer therapy, J. Funct. Biomater. 13 (2022) 196, https://doi.org/10.3390/jfb13040196.
[52] S. Honary, F. Zahir, Effect of zeta potential on the properties of nano-drug delivery systems - a review (Part 2), Trop. J. Pharmaceut. Res. 12 (2013), https://doi.org/10.4314/tjpr.v12i2.20.
[53] E. Blanco, H. Shen, M. Ferrari, Principles of nanoparticle design for overcoming biological barriers to drug delivery, Nat. Biotechnol. 33 (2015) 941–951, https://doi.org/10.1038/nbt.3330.
[54] A. Woźniak, A. Malankowska, G. Nowaczyk, B.F. Grześkowiak, K. Tuśnio, R. Słomski, A. Zaleska-Medynska, S. Jurga, Size and shape-dependent cytotoxicity profile of gold nanoparticles for biomedical applications, J. Mater. Sci. Mater. Med. 28 (2017) 92, https://doi.org/10.1007/s10856-017-5902-y.
[55] J. Polte, Fundamental growth principles of colloidal metal nanoparticles – a new perspective, CrystEngComm 17 (2015) 6809–6830, https://doi.org/10.1039/C5CE01014D.
[56] J.M. Koehler, N. Visaveliya, A. Knauer, Controlling formation and assembling of nanoparticles by control of electrical charging, polarization, and electrochemical potential, Nanotechnol. Rev. 3 (2014), https://doi.org/10.1515/ntrev-2014-0006.
[57] R.S. Riley, E.S. Day, Gold nanoparticle-mediated photothermal therapy: applications and opportunities for multimodal cancer treatment, WIREs Nanomedicine and Nanobiotechnology 9 (2017), https://doi.org/10.1002/wnan.1449.
[58] A.K. Srivastava, R. Yadev, V.N. Rai, T. Ganguly, S.K. Deb, Surface Plasmon Resonance in Gold Nanoparticles, 2012, pp. 305–306, https://doi.org/10.1063/1.4710001.
[59] V. Amendola, R. Pilot, M. Frasconi, O.M. Maragò, M.A. Iatì, Surface plasmon resonance in gold nanoparticles: a review, J. Phys. Condens. Matter 29 (2017) 203002, https://doi.org/10.1088/1361-648X/aa60f3.
[60] S. Peng, J.M. McMahon, G.C. Schatz, S.K. Gray, Y. Sun, Reversing the size-dependence of surface plasmon resonances, Proc. Natl. Acad. Sci. USA 107 (2010) 14530–14534, https://doi.org/10.1073/pnas.1007524107.
[61] P.B. Santhosh, J. Genova, H. Chamati, Green synthesis of gold nanoparticles: an eco-friendly approach, Chemistry (Easton). 4 (2022) 345–369, https://doi.org/10.3390/chemistry4020026.
[62] Z. Hormozi-Moghaddam, A. Neshasteh-Riz, S.M. Amini, S. Aliakbari, P. Hejazi, S. Cheraghi, S.M. Taheri, A. Aghaei, Investigating the effect of low-intensity ultrasound radiation in the presence of Apigenin-coated gold nanoparticles on the expression of mRNAs affecting the apoptosis of MCF7 breast cancer cells, Food Biosci. 57 (2024) 103486, https://doi.org/10.1016/j.fbio.2023.103486.
[63] Z. Sharifiaghdam, S.M. Amini, F. Dalouchi, A.B. Behrooz, Y. Azizi, Apigenin-coated gold nanoparticles as a cardioprotective strategy against doxorubicin-induced cardiotoxicity in male rats via reducing apoptosis, Heliyon 9 (2023) e14024, https://doi.org/10.1016/j.heliyon.2023.e14024.
[64] E. Mohammadi, S.M. Amini, S.H. Mostafavi, S.M. Amini, An overview of antimicrobial efficacy of curcumin-silver nanoparticles, Nanomedicine Res. J. 6 (2021) 105–111, https://doi.org/10.22034/nmrj.2021.02.002.
[65] S.M. Amini, T. Emami, M. Rashidi, H. Zarrinnahad, Curcumin-gold nanoformulation: synthesis, characterizations and biomedical application, Food Biosci. 57 (2024) 103446, https://doi.org/10.1016/j.fbio.2023.103446.
[66] A. Neshastehriz, S.M. Amini, A. Mohammadi, S.R. Mahdavi, V.P. Mahabadi, A. Akbari, In-vitro investigation of green synthesized gold nanoparticle's role in combined photodynamic and radiation therapy of cancerous cells, Adv. Nat. Sci. Nanosci. Nanotechnol. 11 (2020) 045006, https://doi.org/10.1088/2043-6254/abb8c7.
[67] K. Sharma, S. Singh, V. Kumar, S. Singh, S. Datta, D.S. Dhanjal, P. Kaur, J. Singh, Saccharomyces cerevisiae as model organism to study biological activities of nanoparticles, in: Model Org. To Study Biol. Act. Toxic. Nanoparticles, Springer Singapore, Singapore, 2020, pp. 101–115, https://doi.org/10.1007/978-981-15-1702-0_6.
[68] V.T. Anju, B. Siddhardha, M. Dyavaiah, Saccharomyces cerevisiae: model organism to evaluate nanoparticle toxicity, in: Model Org. To Study Biol. Act. Toxic. Nanoparticles, Springer Singapore, Singapore, 2020, pp. 317–332, https://doi.org/10.1007/978-981-15-1702-0_16.
[69] O. Ozbek, K.O. Ulgen, N. Ileri Ercan, The toxicity of polystyrene-based nanoparticles in Saccharomyces cerevisiae is associated with nanoparticle charge and uptake mechanism, Chem. Res. Toxicol. 34 (2021) 1055–1068, https://doi.org/10.1021/acs.chemrestox.0c00468.
[70] C.O. Silva, P. Rijo, J. Molpeceres, I.V. Figueiredo, L. Ascensão, A.S. Fernandes, A. Roberto, C.P. Reis, Polymeric nanoparticles modified with fatty acids encapsulating betamethasone for anti-inflammatory treatment, Int. J. Pharm. 493 (2015) 271–284, https://doi.org/10.1016/j.ijpharm.2015.07.044.
[71] M.H. Hussain, N.F. Abu Bakar, A.N. Mustapa, K.-F. Low, N.H. Othman, F. Adam, Synthesis of various size gold nanoparticles by chemical reduction method with different solvent polarity, Nanoscale Res. Lett. 15 (2020) 140, https://doi.org/10.1186/s11671-020-03370-5.
[72] S. Annur, S.J. Santosa, N. Hidayat Aprilita, pH dependence of size control in gold nanoparticles synthesized at room temperature, Orient. J. Chem. 34 (2018) 2305–2312, https://doi.org/10.13005/ojc/340510.
[73] M. Luty-Błocho, M. Wojnicki, K. Fitzner, Gold nanoparticles formation via Au(III) complex ions reduction with <scp>l</scp> -ascorbic acid, Int. J. Chem. Kinet. 49 (2017) 789–797, https://doi.org/10.1002/kin.21115.
[74] A. Sood, V. Arora, J. Shah, R.K. Kotnala, T.K. Jain, Ascorbic acid-mediated synthesis and characterisation of iron oxide/gold core–shell nanoparticles, J. Exp. Nanosci. 11 (2016) 370–382, https://doi.org/10.1080/17458080.2015.1066514.
[75] M.M. Phiri, D.W. Mulder, B.C. Vorster, Seedless gold nanostars with seed-like advantages for biosensing applications, R. Soc. Open Sci. 6 (2019) 181971, https://doi.org/10.1098/rsos.181971.
[76] L. Zhao, X. Ji, X. Sun, J. Li, W. Yang, X. Peng, Formation and stability of gold nanoflowers by the seeding approach: the effect of intraparticle ripening, J. Phys. Chem. C 113 (2009) 16645–16651, https://doi.org/10.1021/jp9058406.